Negative radiation pressure in Bose-Einstein condensates

Dominik Ciurla,[1,*] Péter Forgács,[2,3] Árpád Lukács,[4,2] and Tomasz Romańczukiewicz[1]
[1]*Institute of Theoretical Physics, Jagiellonian University, Łojasiewicza 11, 30-348 Kraków, Poland*
[2]*Wigner RCP RMI, POB 49, 1525 Budapest, Hungary*
[3]*Institut Denis-Poisson, UMR No. 7013, CNRS, Université de Tours, Parc de Grandmont, 37200 Tours, France*
[4]*Department of Mathematical Sciences, Durham University, Stockton Road, Durham DH1 3LE, United Kingdom*

(Received 7 July 2023; revised 13 December 2023; accepted 2 January 2024; published 30 January 2024)

In two-component nonlinear Schrödinger equations, the force exerted by incident monochromatic plane waves on an embedded dark soliton and on dark-bright-type solitons is investigated, both perturbatively and by numerical simulations. When the incoming wave is nonvanishing only in the orthogonal component to that of the embedded dark soliton, its acceleration is in the opposite direction to that of the incoming wave. This somewhat surprising phenomenon can be attributed to the well-known negative effective mass of the dark soliton. When a dark-bright soliton, whose effective mass is also negative, is hit by an incoming wave nonvanishing in the component corresponding to the dark soliton, the direction of its acceleration coincides with that of the incoming wave. This implies that the net force acting on it is in the opposite direction to that of the incoming wave. This rather counterintuitive effect is a yet another manifestation of negative radiation pressure exerted by the incident wave, observed in other systems. When a dark-bright soliton interacts with an incoming wave in the component of the bright soliton, it accelerates in the opposite direction; hence the force is pushing it now. We expect that these remarkable effects, in particular the negative radiation pressure, can be experimentally verified in Bose-Einstein condensates.

DOI: 10.1103/PhysRevE.109.014228

I. INTRODUCTION

In this paper we consider the interaction of solitons and the sound waves in a two-component, nonlinear Schrödinger equation (NLSE) in one dimension. The NLSE is a widely used model, for example, in nonlinear optics [1], and in particular it serves to describe Bose-Einstein condensates (BECs) of neutral atoms. The motivation of our enterprise is to point out some simple but somewhat surprising physical phenomena, which are hopefully experimentally observable in BECs.

Bose-Einstein condensates were realized experimentally for the first time in [2] and have been produced in numerous experiments ever since. Many BECs can be described in a mean-field approximation, leading to the NLSE, for which classical field-theoretic methods are appropriate. Moreover, in a number of situations, the dynamics of solitons in a BEC can be well approximated by restricting the dynamics to one spatial dimension. Often, the trap used in experiments can be approximated by a harmonic potential, and choosing its frequencies in the two chosen dimensions to be much larger than in the remaining third dimension, an effective, quasi-1D cigar-shaped condensate is achieved [3]. Bose-Einstein condensates with two distinguishable components are described in a mean-field approximation by coupled nonlinear Schrödinger equations (CNLSEs) [4,5]. Experimentally, such two-component BECs can be achieved either by mixing two different atomic species, e.g., ^{41}K and ^{87}Rb [6] ($m_1/m_2 \approx 0.47$), or by using two different spin states of the same species [7]. Although different kinds of solitons can be found in this system (see, e.g., [8,9]), we focus on the so-called dark-bright (DB) and dark solitons.

Dark solitons have been studied theoretically in the context of BEC [10] and subsequently in the context of optical fibers [11]. In particular, their dynamics was researched extensively, including multisoliton interactions [12–14], collisions [15,16], and interactions with perturbations [17–22]. Similarly, dark-bright solitons were a subject of many theoretical articles [4,23–27], together with their generalizations to vortex-bright solitons [28,29], discrete equations [30], and spinor condensates [31]. Dark and dark-bright solitons were realized experimentally both in BECs [32–40] and in nonlinear optics [41–43]. Many reviews of the topic can be found, e.g., [3,44–46].

In the present work we show that in the two-component CNLSE, the interaction of dark and dark-bright solitons with incoming small-amplitude plane waves can be reasonably well described by standard scattering theory. We derive the force acting on the solitons in terms of scattering data. When the amplitude of the plane waves is sufficiently small, linearization about the soliton provides a tractable approximation with good precision. In this case, the waveform is obtained as a solution of the Bogoliubov–de Gennes equations (BdGEs) [47]. The force acting on the soliton can be easily found from momentum conservation. For the case of main interest for us, when an incoming plane wave of amplitude a and wave number k_1 is nonzero only in one component, say, 1 (dark),

*dominik.ciurla@doctoral.uj.edu.pl

then the induced force can be written as

$$F = a^2\big[k_1^2(1+R_1-T_1)+(k_2^+)^2(R_2^+-T_2^+) + (k_2^-)^2(R_2^- - T_2^-)\big], \tag{1}$$

where R_i and T_i denote the transmission and reflection coefficients, respectively, for an incoming wave into channel i and $k_2^\pm$ are the two possible wave numbers in the bright component. In realistic scenarios, for a equal to about 10% of a DB soliton's dark component amplitude, the accelerations due to this force are up to the order of 10^{-2} m/s^2 (see Sec. V D).

We note that the dynamics due to a force acting on dark and dark-bright solitons is somewhat counterintuitive, since the direction of the force and that of the resulting acceleration point in opposite directions because of their effective negative mass.

The value of the coupling g_{12} between the two components of the CNLSE plays an important role, since for $g_{12} = 1$ (in suitable units) the system is integrable [48], and in this special case the net force exerted by incoming waves on solitons is zero. In fact, for the integrable case, exact solutions corresponding to nonlinear superposition of cnoidal waves and solitons have been constructed [49]. We find that quite generally, for $g_{12} \neq 1$ in two-component CNLS systems, an incoming plane wave can exert a pulling force on certain solitons, referred to as the tractor beam effect or negative radiation pressure. As it has been already demonstrated for a number of cases in one and two dimensions, in the presence of two scattering channels with different dispersion relations, an incoming plane wave can exert a pulling force on the scatterer [50].

The paper is organized as follows. We review briefly some of the main properties of two-component CNLSEs in Sec. II A, exhibit the expressions for the energy and field momentum in Sec. II B, and present the linearized equations of motion around a soliton in Sec. II C. In Sec. III we introduce the general notion of the Newtonian approximation using the effective mass and force. We apply these ideas to the specific cases of dark and dark-bright solitons, with a small wave in each component, in Secs. IV and V, respectively. Most importantly, we derive the acceleration of the solitons using an effective model and compare it with numerical simulations of the full CNLSE. In Sec. V D we verify how well the results derived from the homogeneous system apply to a dark-bright soliton in a harmonic trap. We summarize in Sec. VI.

II. MODEL

A. Coupled nonlinear Schrödinger (Gross-Pitaevskii) equation

In the mean-field regime, a one-dimensional two-component Bose–Einstein condensate can be described by two coupled nonlinear Schrödinger equations, also called Gross-Pitaevskii equations, of the form [4,5,35,51–53]

$$i\hbar\partial_t\psi_1 = -\frac{1}{2m_1}\partial_{xx}\psi_1 + (g_{11}|\psi_1|^2 + g_{12}|\psi_2|^2)\psi_1 + V_1(x)\psi_1,$$
$$i\hbar\partial_t\psi_2 = -\frac{1}{2m_2}\partial_{xx}\psi_2 + (g_{22}|\psi_2|^2 + g_{12}|\psi_1|^2)\psi_2 + V_2(x)\psi_2, \tag{2}$$

where ψ_i $(i = 1, 2)$ denote the (complex) wave functions of the two components of the condensate, m_i are their masses, and V_i are the trapping potentials experienced by the ith component. If $m_1 = m_2$, the couplings can be written as $g_{ij} = 2\hbar\omega_\perp a_{ij}$ [35,51–53], where a_{ij} denote the s-wave scattering lengths between the two components (or within one component in the case of a_{ii}) and $\omega_\perp$ is the transverse trapping frequency. The system can be described by the above one-dimensional equations if the frequencies of trapping potentials in the x direction, i.e., $V_i(x)$, are much smaller than $\omega_\perp$. Positive values of a_{ij} (and therefore also of g_{ij}) correspond to repulsive interaction between the components i and j, whereas a negative value corresponds to the interaction being attractive.

In order to simplify the problem, we reduce the number of parameters used. First, we consider a condensate made of two different spin states of the same atomic species; therefore, $m_1 = m_2$, and we can rescale $m_i = 1$. Second, we set $g_{ii} = 1$ and keep g_{12} as a free parameter. The former is justified, because the ratio of scattering lengths in experiments is often close to one, e.g., in the mixture of the $|2, 1\rangle$ and $|1, -1\rangle$ states of ^{87}Rb without additional tuning it is $a_{11}/a_{12}/a_{22} = 1.03/1/0.97$ [7], or for $|1, -1\rangle$ and $|2, -2\rangle$ states $a_{11}/a_{12}/a_{22} = 1.01/1/1$ [33]. Scattering lengths can be manipulated (both their magnitudes and their signs) using Feshbach resonances [54]. In particular, a_{12} can be tuned independently [55–57] and therefore different values of the g_{12} coefficient are achievable in experiments. Finally, we assume that $V_i = 0$, which should be a valid first approximation; we will verify that later in Sec. V D. Therefore, we assume $a_{11} = a_{22}$ and take $m = m_1 = m_2$ as the unit of mass, $\hbar/2a_{11}m\omega_\perp$ as the length unit, and $\hbar/4a_{11}^2m\omega_\perp^2$ as the unit of time. Then the set of equations (2) takes the form

$$i\partial_t\psi_1 = -\tfrac{1}{2}\partial_{xx}\psi_1 + (|\psi_1|^2 + g_{12}|\psi_2|^2)\psi_1,$$
$$i\partial_t\psi_2 = -\tfrac{1}{2}\partial_{xx}\psi_2 + (|\psi_2|^2 + g_{12}|\psi_1|^2)\psi_2. \tag{3}$$

The system of equations (3) has various types of solitonic solutions (see the review in [44]). The simplest solutions correspond to the embedding of a scalar soliton into one of the components. We consider embedded dark solitons, for which the probability density has a dip, and dark-bright (DB) solitons, having a dip and a peak of the probability density in the components ψ_1 and ψ_2, respectively. When $g_{12} = 1$, Eqs. (3) correspond to the Manakov system [48], which is known to be integrable (see also Ref. [58]). For the integrable case, the DB solitons are known analytically, while for values of $g_{12} \neq 1$ we have solved Eqs. (3) numerically. For such values of $g_{12} \neq 1$, we have shown analytically and also confirmed by numerical simulations that incoming sound waves (referred to as radiation) do exert a force on the solitons.

Usually, particlelike objects such as solitons are pushed in the direction of propagation of an incoming wave. However, in some cases the wave pulls a soliton in the opposite direction. We refer to such a situation as negative radiation pressure. In the case of dark and dark-bright solitons, this definition needs an additional clarification. Such solitons have negative effective mass; therefore, their acceleration has an opposite sign to the effective force. Thus, we define a positive (negative) radiation pressure [PRP (NRP)] as a setup in which the force has the same (opposite) sign as (to) the direction of the incoming wave. This means that, in terms of an acceleration of dark and DB solitons, PRP and NRP correspond to a wave pulling and pushing a soliton, respectively. We remark that in the literature on NRP [50,59–63], in the systems considered up to now only positive masses occurred; therefore, the NRP exerted by incident plane waves has manifested by a pulling effect.

B. Integrals of motion

The Lagrangian density corresponding to the CNLSEs (3) is [64]

$$\mathcal{L} = \frac{1}{2}\sum_{i=1,2}[i(\psi_i^*\partial_t\psi_i - \psi_i\partial_t\psi_i^*) - |\partial_x\psi_i|^2 - |\psi_i|^4 - g_{12}|\psi_1|^2|\psi_2|^2]. \tag{4}$$

Using the symmetries of the Lagrangian (4) and the Noether theorem (details in Appendix A), the total energy and momentum are derived as

$$E = \frac{1}{2}\sum_{i=1,2}\int_{-\infty}^{\infty}(|\partial_x\psi_i|^2 + |\psi_i|^4 + g_{12}|\psi_1|^2|\psi_2|^2)\mathrm{d}x, \tag{5}$$

$$P = \frac{i}{2}\sum_{i=1,2}\int_{-\infty}^{\infty}(\psi_i\partial_x\psi_i^* - \psi_i^*\partial_x\psi_i)\mathrm{d}x, \tag{6}$$

and it is shown that they obey the equations

$$\partial_t E = \frac{1}{2}\sum_{i=1,2}(\partial_x\psi_i^*\partial_t\psi_i + \partial_x\psi_i\partial_t\psi_i^*)|_{-\infty}^{\infty}, \tag{7}$$

$$\partial_t P = \frac{1}{2}\sum_{i=1,2}[-i(\psi_i^*\partial_t\psi_i - \psi_i\partial_t\psi_i^*) - |\partial_x\psi_i|^2 + |\psi_i|^4 + g_{12}|\psi_1|^2|\psi_2|^2]|_{-\infty}^{\infty}. \tag{8}$$

It is also worth noting that, due to the $U(1)\times U(1)$ symmetry, the solutions of Eqs. (3) obey the continuity equations (even if we include the trapping potential)

$$\partial_t|\psi_i|^2 + \partial_x J_i = 0, \tag{9}$$

where

$$J_i = \frac{i}{2}(\psi_i\partial_x\psi_i^* - \psi_i^*\partial_x\psi_i). \tag{10}$$

Note that $P = \sum_{i=1,2}\int_{-\infty}^{\infty} J_i\,\mathrm{d}x$. Integrating Eq. (9) over the whole space and using the Newton-Leibniz theorem, we obtain

$$\partial_t\int_{-\infty}^{\infty}|\psi_i|^2\mathrm{d}x = -J_i|_{-\infty}^{\infty}. \tag{11}$$

We can choose the normalization as $\int|\psi_i(x,t)|^2\mathrm{d}x = N_i$, where N_i is the number of atoms in the ith component. These particle numbers are conserved.

C. Linearization around a soliton

We consider stationary solitons of Eqs. (3) of the form $\psi_i(x,t) = e^{-i\mu_i t}\Phi_i(x)$, where $\Phi_i(x)$ are real functions satisfying the following equations:

$$\mu_1\Phi_1 = -\tfrac{1}{2}\partial_{xx}\Phi_1 + (|\Phi_1|^2 + g_{12}|\Phi_2|^2)\Phi_1,$$
$$\mu_2\Phi_2 = -\tfrac{1}{2}\partial_{xx}\Phi_2 + (|\Phi_2|^2 + g_{12}|\Phi_1|^2)\Phi_2. \tag{12}$$

If the wave function is normalized to the number of atoms in each component, then the μ_i are determined from these normalization conditions and they are interpreted as chemical potentials [65].

Let us consider a small perturbation of a soliton solution of Eqs. (3), of the form

$$\psi_i(x,t) = e^{-i\mu_i t}[\Phi_i(x) + a\xi_i(x,t)], \tag{13}$$

where the parameter of the perturbation $a \ll 1$. Moreover, let us make an ansatz

$$\xi_i(x,t) = e^{i\tilde{\omega}t}\xi_i^+(x) + e^{-i\tilde{\omega}t}\xi_i^-(x). \tag{14}$$

After inserting this ansatz into Eqs. (3) and keeping only terms linear in a, we obtain that ξ_i^- and ξ_i^+ satisfy

$$\left(-\tfrac{1}{2}\partial_{xx} + \mathbf{M}\right)\Xi = \mathrm{diag}(\mu_1+\tilde{\omega}, \mu_1-\tilde{\omega}, \mu_2 + \tilde{\omega}, \mu_2-\tilde{\omega})\Xi, \tag{15}$$

where diag means diagonal matrix, Ξ stands for the vector

$$\Xi = (\xi_1^-, \xi_1^{+*}, \xi_2^-, \xi_2^{+*})^{\mathrm{T}}, \tag{16}$$

and

$$\mathbf{M} = \begin{pmatrix} 2\Phi_1^2 + g_{12}\Phi_2^2 & \Phi_1^2 & g_{12}\Phi_1\Phi_2 & g_{12}\Phi_1\Phi_2 \\ \Phi_1^2 & 2\Phi_1^2 + g_{12}\Phi_2^2 & g_{12}\Phi_1\Phi_2 & g_{12}\Phi_1\Phi_2 \\ g_{12}\Phi_1\Phi_2 & g_{12}\Phi_1\Phi_2 & g_{12}\Phi_1^2 + 2\Phi_2^2 & \Phi_2^2 \\ g_{12}\Phi_1\Phi_2 & g_{12}\Phi_1\Phi_2 & \Phi_2^2 & g_{12}\Phi_1^2 + 2\Phi_2^2 \end{pmatrix}. \tag{17}$$

Equation (15) is the generalization of the BdGE [47] to the two-component CNLSE. Here we consider plane-wave solutions of Eq. (15), but also note that the existence of bound-state solutions with complex $\tilde{\omega}$ would signal instability of the soliton. Such stability analyses have been performed, e.g., in Refs. [4,45] in similar coupled models, and in Refs. [66–68] for a single-component NLSE. In our case, the numerical technique used for finding the soliton (gradient descent) already ensures that unstable solitons are not found.

We consider a setup consisting of a soliton and a wave. The wave is incoming from $-\infty$ in one of the two components of the BEC and is moving to the right. It corresponds to Eq. (13) with a interpreted as the amplitude (and the appropriate boundary conditions discussed later). Using the linearization described above, the wave can be written as

$$ae^{-i\mu_i t}\xi_i(x,t) = ae^{-i(\mu_i-\tilde{\omega})t}\xi_i^+(x) + ae^{-i(\mu_i+\tilde{\omega})t}\xi_i^-(x) \quad (18)$$

and we can define its frequencies as

$$\omega_i^{\pm} = \mu_i \mp \tilde{\omega}, \quad (19)$$

which correspond to those on the right-hand side of Eq. (15). Sometimes we loosely refer to $\tilde{\omega}$ as the frequency, but the true frequencies of the wave are given by $\omega_i^{\pm}$. We assume that asymptotically these waves have a form of monochromatic plane waves. We define transmission and reflection coefficients, separately for each of the examples, as coefficients of the asymptotic plane-wave modes in a solution.

III. NEWTONIAN MOTION AND THE EFFECTIVE MASS OF SOLITONS

We expect both the dark and the dark-bright solitons of the NLSE to behave as Newtonian particles in the first approximation, albeit with unusual dynamics, due to their negative effective masses. In this present context, we refer the reader to Ref. [69] for the motion of dark solitons, and for a recent review of the dynamics of solitons in the vector NLSE see Ref. [45].

More precisely, we assume that in the presence of perturbations, the solitons do not change their shape and that we can treat the center of the soliton x_0 solely as a function of time, reducing the problem to one-dimensional classical dynamics. In this description, $x_0(t)$ is expected to obey the equation

$$M\ddot{x}_0(t) = F, \quad (20)$$

where M and F are the effective mass and force, respectively. These quantities are obtained from the integrals of motion discussed in Sec. II B. The description of the dynamics of the dark soliton is complicated by the fact that the wave function describes the soliton on top of a constant background [69].

The energy E and the momentum P of the dark soliton have to be defined carefully; they have to be renormalized in order to subtract the contribution from the background [17,44]. The renormalized quantities P_s and E_s will be given separately for the dark and dark-bright soliton (see Secs. IV and V).

A useful definition of the effective mass M from the renormalized total energy E_s and momentum P_s for a soliton moving with velocity v is given as

$$M = \left.\frac{\mathrm{d}^2E_s}{\mathrm{d}v^2}\right|_{v=0} = \left.\frac{\mathrm{d}P_s}{\mathrm{d}v}\right|_{v=0}. \quad (21)$$

If the soliton is indeed moving according to Newton's law, M computed from E_s should match that derived from P_s.

The effective force exerted by the sound waves on the soliton can be obtained as the time derivative of the total momentum $\partial_t P$. Since the renormalization corrections are time independent, $\partial_t P = \partial_t P_s$. We are interested in the force averaged over a period of the incoming wave; thus we are led to define the effective force as

$$F = \langle \partial_t P\rangle_T, \quad (22)$$

where P is the total momentum including the radiation and $\langle\cdot\rangle_T$ is the average over a period. We note that to evaluate Eq. (8) it is sufficient to know the asymptotic form of the radiation in order to compute the effective force. In the computation of F, we can only keep the contributions of order a^2 since we have the solution up to linear order in the amplitude. In this linearized approximation (which turns out to be quite efficient), one can easily obtain the results for any incoming waveform.

IV. DARK SOLITON

A. Dark soliton solution

A particular solution of Eq. (3) with arbitrary g_{12} is a (scalar) dark soliton centered at x_0 [4], embedded into the vector NLSE

$$\psi_1 = e^{-i\mu t}\sqrt{\mu}\tanh[\sqrt{\mu}(x-x_0)], \quad \psi_2 = 0, \quad (23)$$

with chemical potential $\mu_1 = \mu > 0$. Such a soliton can be understood as a dip in the probability density obtained from the collective wave function of atoms in the condensate. We consider two scenarios: In the first case the additional atoms will be present in the second component in the form of a plane wave (a system still described by the two-component model) and in the second case the second component will be completely absent (a problem reduced to the one-component NLSE).

In order to examine the effective force exerted by an incoming plane wave on a dark soliton, we need to analyze the linearized equations. The relation between $\tilde{\omega}$ (see Sec. II C) and the wave numbers k_i is obtained from the $x \to \pm\infty$ asymptotic form of Eq. (15). Knowing that $\Phi_1(x) \to \pm\sqrt{\mu}$ and $\Phi_1''(x) \to 0$ as $x \to \pm\infty$, the asymptotic form of the matrix from Eq. (17) is

$$\mathbf{M}_{x\to\pm\infty} = \mu\begin{pmatrix} 2 & 1 & 0 & 0 \\ 1 & 2 & 0 & 0 \\ 0 & 0 & g_{12} & 0 \\ 0 & 0 & 0 & g_{12} \end{pmatrix}. \quad (24)$$

The linearized equations (15) with this $\mathbf{M}$ can easily be diagonalized and solved, obtaining

$$\xi_1^-(x) = Ae^{ik_1x} + Be^{-ik_1x},$$
$$\xi_1^+(x) = \left(-\frac{\frac{k_1^2}{2}-\tilde{\omega}}{\mu} - 1\right)(A^*e^{-ik_1x} + B^*e^{ik_1x}), \quad (25)$$

where A and B are arbitrary constants and

$$k_1 = \sqrt{2}\sqrt{\sqrt{\mu^2+\tilde{\omega}^2} - \mu}. \quad (26)$$

In the above solution we omitted the solutions with imaginary wave number, since they describe nonpropagating solutions and therefore do not carry a momentum. Note that for $\tilde{\omega} \neq 0$ the wave number k_1 is real; thus Eqs. (25) describe propagating (traveling) waves.

As mentioned earlier, we consider waves coming from the left and moving to the right. The direction of the traveling wave is determined by a relative sign of the wave frequency and its wave vector. Assuming an incoming wave with e^{ik_1x} for ω_1^+ and (to be consistent with the above solution) e^{-ik_1x} for ω_1^-, the condition for moving to the right is that the frequency

$\omega_1^{\pm} = \mu \mp \tilde{\omega}$ is positive or negative, respectively [cf. Eqs. (18) and (19)]. This can be transformed into the following conditions for $\tilde{\omega}$: $\tilde{\omega} < \mu$ for ω_1^+ and $\tilde{\omega} < -\mu$ for ω_1^-. Therefore, for $\tilde{\omega} < -\mu$ both waves propagate to the right.

In the second component, the equations are already diagonal. Note that in this case μ_2 is arbitrary and choosing it can be interpreted as fixing a reference point for $\tilde{\omega}$. For simplicity, let us set $\mu_2 = 0$; then we can interpret $\mp\tilde{\omega} = \omega_2^{\pm}$ simply as the frequency of the incoming wave in the second sector. Then the solutions are

$$\xi_2^-(x) = Ce^{ik_2^- x} + De^{-ik_2^- x},$$
$$\xi_2^+(x) = Ee^{ik_2^+ x} + Fe^{-ik_2^+ x}, \tag{27}$$

where

$$k_2^{\pm} = \sqrt{2}\sqrt{\mp\tilde{\omega} - \mu g_{12}} \tag{28}$$

and $C, D, E,$ and F are arbitrary constants. These waves propagate when $k_2^{\pm}$ is real (and nonzero), that is, when $\mp\tilde{\omega} > \mu g_{12}$. This means that for $g_{12} < 0$ there exists a range of $\tilde{\omega}$ in which both waves can propagate with the same $\tilde{\omega}$ and for $g_{12} \geqslant 0$ with fixed $\tilde{\omega}$ only one (or neither) of the waves can propagate.

Let us analyze how the parameter $\tilde{\omega}$ affects the direction of propagation of the waves in the second component. Using the same logic as for the first component (assuming an incoming wave with $e^{ik_2^{\pm} x}$), we get the conditions for the range of $\tilde{\omega}$ in which the waves in the second component are moving to the right, namely, we obtain $\tilde{\omega} < 0$ for ω_2^+ and $\tilde{\omega} > 0$ for ω_2^-. This means that only one of them moves to the right for a given $\tilde{\omega}$.

In order to find the effective mass of the soliton, we repeat the derivation of the renormalized momentum done in [17] (for additional details see also [70]) and obtain the effective mass from it following [44]. First, we consider the total momentum P_s of a scalar dark soliton moving with a constant velocity v (often called the gray soliton):

$$\psi_1 = e^{-i\mu t}\{iv + \sqrt{\mu - v^2}\tanh[\sqrt{\mu - v^2}(x - x_0 - vt)]\},$$
$$\psi_2 = 0. \tag{29}$$

Note that the moving soliton becomes shallower and shallower as the velocity increases, finally vanishing when $v^2 = \mu$, which defines its maximal velocity. However, the above wave function describes a dark soliton on top of a background, and we are interested in the total momentum of the soliton. Let us note that the solution with constant probability density, corresponding to the asymptotics of (29), i.e., $|\psi_1|^2 = \mu$ and $|\psi_2|^2 = 0$, is of the form

$$\psi_1 = \sqrt{\mu}e^{-i(\mu + q^2/2)t}e^{iqx},$$
$$\psi_2 = 0, \tag{30}$$

with some real q. Since we are interested in a nonmoving background, we choose $q = 0$, yielding the background part of the dark soliton. However, we have to take into account the phase change induced by the presence of the soliton (see [17]). Therefore, we assume that the background (in the first component) has the form

$$\psi_b = \sqrt{\mu}e^{-i\mu t}e^{ik(x)x}, \tag{31}$$

where k is some real function of x, reflecting the phase change induced by a soliton. It will turn out that the explicit form of $k(x)$ is not needed. Although the probability density of the background is constant (equal to μ), the total momentum contribution also depends on the phase. Inserting Eq. (31) into Eq. (6) we obtain that the contribution of the background can be written as

$$\mu\Delta\phi \equiv \mu\int_{-\infty}^{\infty}[k(x) + xk'(x)]\mathrm{d}x = \mu xk(x)_{-\infty}^{\infty}. \tag{32}$$

Comparing with Eq. (31), $\Delta\phi$ is readily identified with the induced phase change of the background. Therefore, the total momentum of the pure soliton can be expressed as (cf. [17,44])

$$P_s = \frac{i}{2}\int_{-\infty}^{\infty}(\psi_1\partial_x\psi_1^* - \psi_1^*\partial_x\psi_1)\mathrm{d}x - \mu\Delta\phi. \tag{33}$$

The phase change $\Delta\phi$ can be easily computed from the asymptotics of Eq. (29):

$$\Delta\phi = -2\arctan\left(\frac{\sqrt{\mu - v^2}}{v}\right). \tag{34}$$

Using this, we obtain from Eq. (33) the momentum corresponding to the soliton

$$P_s = -2v\sqrt{\mu - v^2} + 2\mu\arctan\left(\frac{\sqrt{\mu - v^2}}{v}\right), \tag{35}$$

which allows us to compute its effective mass as (cf. [44])

$$M = \left.\frac{dP_s}{dv}\right|_{v\to 0} = -4\sqrt{\mu}. \tag{36}$$

Intuitively, the negative sign is not a surprise, because a dark soliton is, as mentioned before, a dip in the collective probability density of atoms. The same mass is obtained using the renormalized energy [17] (see Sec. III)

$$E_s = \frac{1}{2}\int_{-\infty}^{\infty}[|\partial_x\psi_1|^2 + (|\psi_1|^2 - \mu)^2]\mathrm{d}x. \tag{37}$$

B. Wave in the second component

Let us now consider the interaction of an embedded dark soliton in the first component and an incoming wave in the second one. In this case one can obtain the analytic solutions of the linearized equations for the waveform in the second component. Since in the case of an embedded dark soliton [Eq. (23)] the linearized equations (15) for ξ_1 and ξ_2 are decoupled from each other, we may simply set $\xi_1 = 0$. Then Eq. (15) is reduced to

$$-\tfrac{1}{2}\partial_{xx}\xi_2^-(x) + g_{12}\mu\tanh^2(\sqrt{\mu}x)\xi_2^-(x) = \tilde{\omega}\xi_2^-(x),$$
$$-\tfrac{1}{2}\partial_{xx}\xi_2^+(x) + g_{12}\mu\tanh^2(\sqrt{\mu}x)\xi_2^+(x) = -\tilde{\omega}\xi_2^+(x). \tag{38}$$

Regular solutions of Eq. (38) can be expressed in terms of associated Legendre functions of the first kind

$$\xi_2^{\pm}(x) = AP_\lambda^{ik_2^{\pm}/\sqrt{\mu}}[\tanh(\sqrt{\mu}x)], \tag{39}$$

where $\lambda = \frac{1}{2}(\sqrt{1 + 8g_{12}} - 1)$ and A is a normalization factor.

Since our boundary conditions correspond to a wave coming from $x = -\infty$, we impose the following asymptotic behavior on ξ_2:

$$\xi_2^{\pm}(x) \xrightarrow[x\to-\infty]{} e^{ik_2^{\pm}x} + r_2^{\pm}e^{-ik_2^{\pm}x},$$
$$\xi_2^{\pm}(x) \xrightarrow[x\to+\infty]{} t_2^{\pm}e^{ik_2^{\pm}x}. \tag{40}$$

This asymptotic behavior can be ensured by choosing the normalization constant A in Eq. (39) appropriately. The reflection and transmission coefficients are defined as $R_2^{\pm} = |r_2^{\pm}|^2$ and $T_2^{\pm} = |t_2^{\pm}|^2$, respectively, and can be written as

$$R_2^{\pm} = \frac{2\sin^2(\pi\lambda)}{\cosh\left(\frac{2\pi k_2^{\pm}}{\sqrt{\mu}}\right) - \cos(2\pi\lambda)},$$
$$T_2^{\pm} = \frac{2\sinh^2\left(\frac{\pi k_2^{\pm}}{\sqrt{\mu}}\right)}{\cosh\left(\frac{2\pi k_2^{\pm}}{\sqrt{\mu}}\right) - \cos(2\pi\lambda)}. \tag{41}$$

One can check that the following relation is satisfied:

$$R_2^{\pm} + T_2^{\pm} = 1. \tag{42}$$

Note that the reflection coefficient is zero not only for $g_{12} = 1$, but for any value of g_{12} such that λ is an integer.

We now investigate the dynamics of a dark soliton embedded in the first component under the influence of an incident plane wave coming from $x = -\infty$ embedded in the second component. We stick to the linearized approximation and we assume the amplitude of the wave a to be sufficiently small. Let us consider the setup in which $\tilde{\omega}$ is such that only one of the waves $\xi_2^{\pm}$ has a real wave number. Then we can omit the other one (ξ_2^{+} or ξ_2^{-}), since it describes a nonpropagating solution and does not carry a momentum. In terms of full wave functions ψ_i, this setup has the following asymptotics:

$$\psi_1(x,t) \xrightarrow[x\to-\infty]{} -\sqrt{\mu}e^{-i\mu t},$$
$$\psi_1(x,t) \xrightarrow[x\to+\infty]{} \sqrt{\mu}e^{-i\mu t},$$
$$\psi_2(x,t) \xrightarrow[x\to-\infty]{} ae^{-i\omega_2^{\pm}t}(e^{ik_2^{\pm}x} + r_2^{\pm}e^{-ik_2^{\pm}x}),$$
$$\psi_2(x,t) \xrightarrow[x\to+\infty]{} ae^{-i\omega_2^{\pm}t}t_2^{\pm}e^{ik_2^{\pm}x}. \tag{43}$$

In order to approximate the acceleration of the soliton, we assume Newtonian motion, with the force stemming from the radiation pressure, averaged over a period of the incoming wave.

The force is derived from Eq. (8). First, we substitute the above asymptotic form into this equation. Then we average it over time for the period $T = 2\pi/\tilde{\omega}$ (which in this case does not change anything) and omit the terms of the order higher than a^2 (since a is small). Finally, we replace $\tilde{\omega}$ with the appropriate dispersion relation with $k_2^{\pm}$, derived in the preceding section, obtaining the force

$$F = \langle\partial_t P\rangle_T = a^2(k_2^{\pm})^2(1 + R_2^{\pm} - T_2^{\pm}), \tag{44}$$

where P is the total momentum and $\langle\cdot\rangle_T$ means the average over the period. Using the relation (42), the force can be simplified to $F = 2a^2(k_2^{\pm})^2R_2^{\pm}$; therefore, in this case reflectionlessness implies no force (of the assumed order a^2).

Let us briefly consider the range of $\tilde{\omega}$ for which ξ_2^{+} and ξ_2^{-} are both traveling waves. Then the initial wave $\xi_2^{\pm}$ can scatter into both ξ_2^{+} and ξ_2^{-} and the analogous derivation leads to the force

$$F = a^2[(k_2^{\pm})^2 + (k_2^{+})^2(\tilde{R}_2^{+} - \tilde{T}_2^{+}) + (k_2^{-})^2(\tilde{R}_2^{-} - \tilde{T}_2^{-})], \tag{45}$$

where the incoming wave has a wave number $k_2^{\pm}$. However, after considering the boundary conditions, $\tilde{R}_2^{\pm}$ and $\tilde{T}_2^{\pm}$ are equal to $R_2^{\pm}$ and $T_2^{\pm}$ from Eq. (41) only for the incoming wave and for the other one are equal to zero. Therefore, the above expression ultimately reduces to Eq. (44). If both are the incoming waves, only one of them is moving to the right for given $\tilde{\omega}$ (see the discussion in Sec. IV A) and also the effective force is simply a sum of individual forces, so it is not interesting at this point.

Finally, using the reflection coefficient given by Eq. (41), the mass derived in the preceding section, and the above F, we can derive the explicit form of acceleration exerted on the scalar dark soliton in the first component by a wave with frequency $\tilde{\omega}$ in the second component. For the incoming wave with a wave number $k_2^{\pm}$ it is

$$\ddot{x}_0 = -\frac{a^2}{\sqrt{\mu}}\frac{(k_2^{\pm})^2\sin^2(\pi\lambda)}{\cosh\left(\frac{2\pi k_2^{\pm}}{\sqrt{\mu}}\right) - \cos(2\pi\lambda)}, \tag{46}$$

where x_0 is interpreted as the position of the soliton. Note that although the force (44) is always non-negative, the acceleration is always nonpositive due to the negative effective mass (36); therefore, we observe either the positive radiation pressure, i.e., positive force, or no pressure at all.

To verify the above results, we performed numerical simulations. The initial condition was a dark soliton in the first sector and a wave propagating from the left end of the interval with a given frequency and an appropriate wave number, where its amplitude was kept sufficiently small. However, the initial wave was multiplied by a superposition of hyperbolic tangents to cut it smoothly, in order to have the initial wave beginning slightly after the left boundary and ending slightly before the center of the soliton. This deviation from a plane-wave shape introduces a short kick exerted on the soliton and this results in a constant velocity, on top of which we observe the acceleration compared with Eq. (46). More precisely, the wave in the second component had the form

$$\psi_2(x, t=0) = ae^{ik_2^{+}x}\Phi_{\text{cut}}(x), \tag{47}$$

with parameters such that a wave with k_2^{+} propagates to the right, i.e., $\tilde{\omega} < 0$ and $\tilde{\omega} < -\mu g_{12}$. Here Φ_{cut} is the cutting function mentioned before,

$$\Phi_{\text{cut}}(x) = \tfrac{1}{2}[\tanh(x - x_{\min} - 10) - \tanh(x + 10)], \tag{48}$$

where $x_{\min}$ is the left boundary in space. The center of the soliton was computed as the minimum of the probability density in the first component. Then the acceleration was computed by fitting the quadratic function to the position of the center and compared with Eq. (46) (see Figs. 1–4). It turned out that our effective linearized model explains the observed accelerations quite well for a wide range of parameters.

C. Dark soliton and a wave in the same component

Since the linearized equations (15) for ξ_1 and ξ_2, in the case of the dark soliton, are independent, we start with a similar ansatz as before, namely, $\xi_2 = 0$. Now we examine the case where the wave with small amplitude a comes from $-\infty$ in

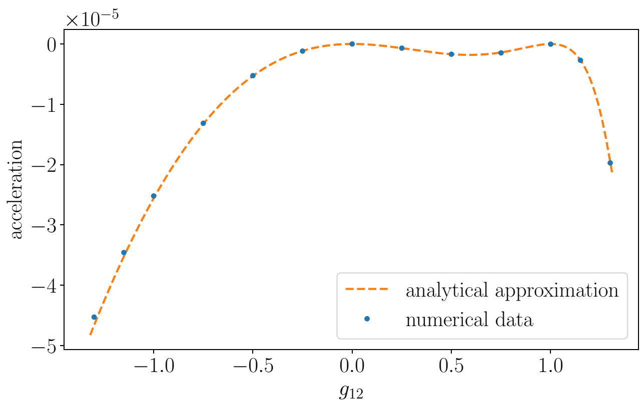

FIG. 1. Acceleration of a dark soliton with $\mu = 1$ under the influence of the wave in the second component coming from the left with a frequency $\omega_2^+ = -\tilde{\omega} = 1.4$ and amplitude $a = 0.05$ for different values of g_{12}.

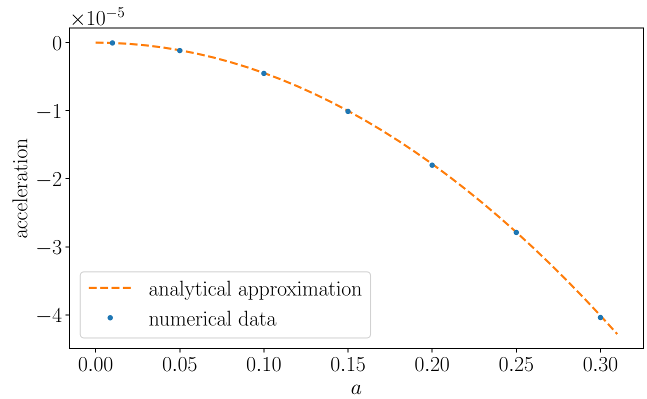

FIG. 3. Acceleration of a dark soliton with $\mu = 1$ under the influence of the wave in the second component coming from the left with a frequency $\omega_2^+ = -\tilde{\omega} = 1.4$, $g_{12} = 0.8$, and different amplitudes.

the first component, which [taking into account the solution (25)] has the asymptotics

$$
\begin{aligned}
\psi_1(x,t) &\xrightarrow[x\to-\infty]{} a\beta\left(-\frac{\frac{k_1^2}{2}-\tilde{\omega}}{\mu}-1\right)e^{-i\omega_1^+ t}\left(e^{ik_1x}+r_1e^{-ik_1x}\right)\\
&\quad + a\beta e^{-i\omega_1^- t}\left(e^{-ik_1x}+r_1^*e^{ik_1x}\right)-\sqrt{\mu}e^{-i\mu t},\\
\psi_1(x,t) &\xrightarrow[x\to+\infty]{} a\beta\left(-\frac{\frac{k_1^2}{2}-\tilde{\omega}}{\mu}-1\right)e^{-i\omega_1^+ t}t_1e^{ik_1x}\\
&\quad + a\beta e^{-i\omega_i^- t}t_1^*e^{-ik_1x}+\sqrt{\mu}e^{-i\mu t},\\
\psi_2(x,t) &\xrightarrow[x\to\pm\infty]{} 0,
\end{aligned}
\tag{49}
$$

where

$$
\beta = \frac{\sqrt{2}\mu}{\sqrt{\left(k_1^2+2\mu\right)\left[k_1\left(\sqrt{k_1^2+4\mu}+k_1\right)+2\mu\right]}}
\tag{50}
$$

is a normalization constant. The reflection and transmission coefficients are defined as $R_1 = |r_1|^2$ and $T_1 = |t_1|^2$, respectively. The coefficient β was chosen in such a way as to have the simplest form of the force. From the above asymptotics, the effective force acting on a soliton can be derived analogously as in the previous case, obtaining

$$
F = a^2k_1^2(1+R_1-T_1).
\tag{51}
$$

The solutions to the linearized equations (15) in this case with $\mu = 1$ can be found in [71–73]. Assuming the asymptotics (49) and transforming them for arbitrary μ, we obtain

$$
\begin{aligned}
\xi_1^{\pm}(x) &= \frac{2\beta k_1}{\left(k_1 \mp 2i\sqrt{\mu}\right)\left(k_1^2+2\tilde{\omega}\right)}\left[\left(\frac{k_1^2}{2}\mp\tilde{\omega}\right)\right.\\
&\quad\left.\times\left(1\pm\frac{2i\sqrt{\mu}}{k_1}\tanh(x\sqrt{\mu})\right)+\frac{\mu}{\cosh^2(x\sqrt{\mu})}\right]e^{\pm ik_1x},
\end{aligned}
\tag{52}
$$

where β is given in (50). The solutions imply $R_1 = 0$ and $T_1 = 1$ and thus no force. However, we also solved the equations numerically, in order to show the more general method used later in this article. The infinities were approximated by sufficiently large L; then $x \in [-L, L]$ [in general, the grid is different from the one used in the full partial differential equation (PDE) simulations of CNLSEs]. We changed the basis from (ξ_1^-, ξ_1^{+*}) to the solutions for which the asymptotic form of the equations (15) is diagonal. Let us denote the solutions

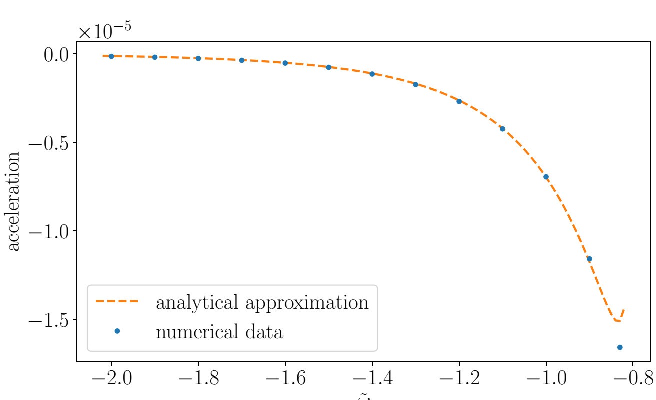

FIG. 2. Acceleration of a dark soliton with $\mu = 1$ under the influence of the wave in the second component coming from the left with different frequencies $\omega_2^+ = -\tilde{\omega}$, $g_{12} = 0.8$, and amplitude $a = 0.05$.

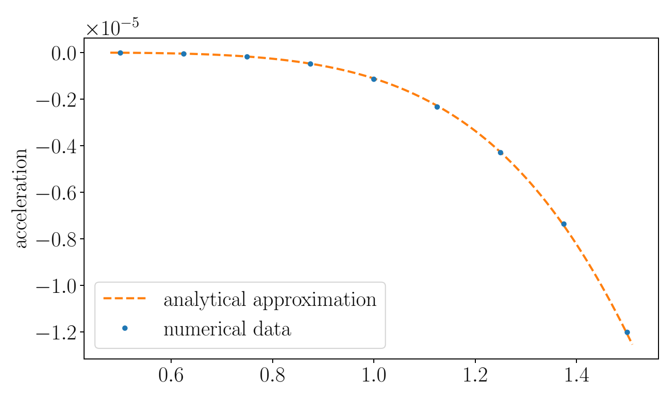

FIG. 4. Acceleration of a dark soliton with different values of μ under the influence of the wave in the second component coming from the left with a frequency $\omega_2^+ = -\tilde{\omega} = 1.4$, $g_{12} = 0.8$, and amplitude $a = 0.05$.

in the new basis by $(\tilde{\xi}_1^-, (\tilde{\xi}_1^+)^*)$. Then the boundary conditions were imposed as

$$(\tilde{\xi}_1^{-\prime} - ik_1\tilde{\xi}_1^-)|_{x=-L} = -2ik_1 e^{ik_1 L} \tag{53}$$

to have $e^{-ik_1 x}$ at $x = -L$ and

$$(\tilde{\xi}_1^{-\prime} + ik_1\tilde{\xi}_1^-)|_{x=L} = 0 \tag{54}$$

to ensure that there is no $e^{ik_1 x}$ at $x = L$. This corresponds to the incoming wave with $e^{ik_1 x}$ for ω_1^+ moving from left to right. Here $(\tilde{\xi}_1^+)^*$ describes the nonpropagating waves and we imposed analogous boundary conditions on it,

$$\begin{aligned}\{[(\tilde{\xi}_1^+)^*]' - ik_{\rm im}(\tilde{\xi}_1^+)^*\}\,|_{x=-L} &= \{[(\tilde{\xi}_1^+)^*]' + ik_{\rm im}(\tilde{\xi}_1^+)^*\}|_{x=L}\\ &= 0,\end{aligned} \tag{55}$$

with imaginary $k_{\rm im} = \pm\sqrt{2}i\sqrt{\sqrt{\mu^2+\tilde{\omega}^2}+\mu}$ instead of k_1. Then R_1 and T_1 were computed from the numerical solutions, using the equations

$$\begin{aligned}R_1 &= |\tilde{\xi}_1^-(-L) - e^{-ik_1 L}|^2,\\ T_1 &= |\tilde{\xi}_1^-(L)|^2.\end{aligned} \tag{56}$$

The acceleration, computed from the force (51) with numerically obtained R_1 and T_1 and the mass derived in the previous section, turned out to be close to zero, as expected.

The above result can be compared with the full PDE simulations of CNLSEs. Before we do that, let us discuss a particular difficulty present here. In the case of a scalar dark soliton with a wave in the second component, determining the center of the soliton from numerical data is relatively easy since the wave and the soliton are in completely different components. Then the center is simply given by a minimum of the probability density in the soliton component. In general, this is not the case because in many scenarios the waves scatter into both components of the condensate. Therefore, developing the strategy of extracting the position of a soliton from numerical data will be important not only for the waves initially in the first component, but for most other setups as well.

When a wave is present in the same component as the soliton, one can observe oscillations of the minimum (in the case of a bright soliton, the maximum) of the probability density. These oscillations are due to the effect of the incident wave on the soliton (cf. Figs. 5 and 16). This interesting effect is the analog described by the Quist effect [74] for vortices. In the present case it complicates the extraction of the position of the soliton from numerical data. To improve the determination of the soliton positions, we used filtering of high frequencies from $|\psi(x,t)|^2$ at each instant t before computing the minimum. Since the amplitude of these oscillations becomes smaller than the observed trajectories during the time evolution, it pays off to make the time evolution as long as feasible.

The initial condition in the numerical simulations was $\psi_2(x, t = 0) = 0$ and

$$\begin{aligned}\psi_1(x, t=0) = \Phi(x) + a\beta\left[\left(-\frac{\frac{k_1^2}{2}-\tilde{\omega}}{\mu} - 1\right)e^{ik_1 x} + e^{-ik_1 x}\right]\\ \times\,\Phi_{\rm cut}(x),\end{aligned} \tag{57}$$

where Φ is the dark soliton for $t = 0$, $\Phi_{\rm cut}$ is the same cutting function as in (48), and β is the normalization given by (50). We used $\tilde{\omega} < -\mu$ in order to have both $e^{\pm ik_1 x}$ starting a wave

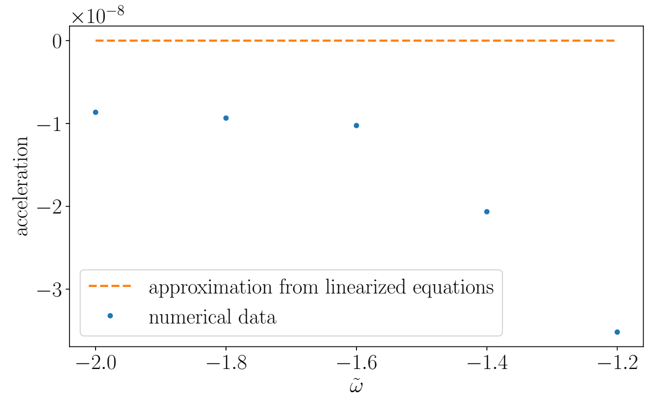

FIG. 6. Acceleration of a dark soliton with $\mu = 1$ under the influence of the wave in the first component coming from the left with different frequencies $\omega_1^\pm = \mu \mp \tilde{\omega}$ and amplitude $a = 0.05$.

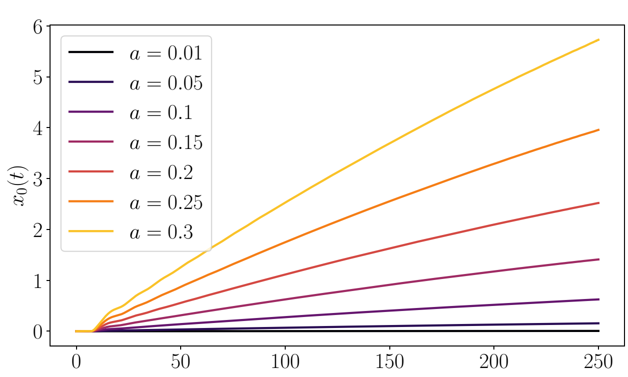

FIG. 5. Position of a dark soliton with $\mu = 1$ under the influence of the wave in the second component coming from the left with a frequency $\omega_2^+ = -\tilde{\omega} = 1.4$, $g_{12} = 0.8$, and different amplitudes.

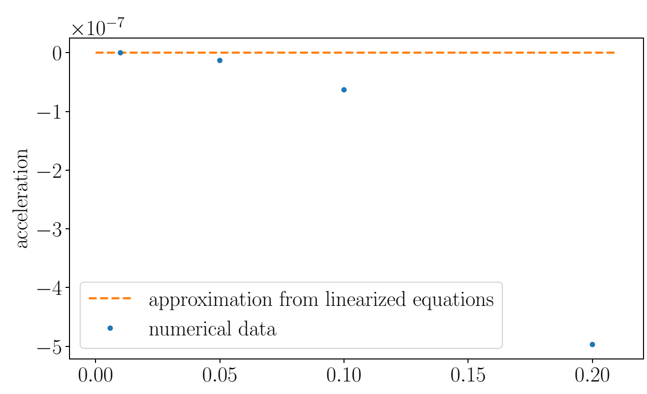

FIG. 7. Acceleration of a dark soliton with $\mu = 1$ under the influence of the wave in the first component coming from the left with frequencies $\omega_1^+ = 2.4$ and $\omega_1^- = -0.4$ (i.e., $\tilde{\omega} = -1.4$), $g_{12} = 0.8$, and different amplitudes.

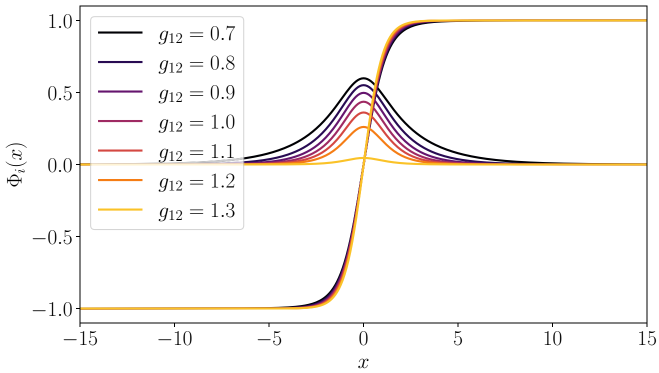

FIG. 8. Dark-bright solitons for different values of the parameter g_{12}, calculated using the gradient flow method. The parameters are $\mu = 1$, $\kappa = 0.9$, and μ_i as given in Eq. (59).

moving to the right. Acceleration computed from Eq. (51) divided by the appropriate effective mass with numerically obtained reflection and transmission coefficients has values close to zero. It was compared with the acceleration from the full PDE simulations (Figs. 6 and 7), which is also small. This seems to indicate that the force is indeed approximately zero.

V. DARK-BRIGHT SOLITONS

A. Dark-bright solutions

The CNLSE (3) with $g_{12} = 1$ possesses a particular solution [23]

$$\psi_1 = e^{-i\mu t}\sqrt{\mu}\tanh[\kappa(x - x_0)],$$
$$\psi_2 = e^{-i(\mu-\kappa^2/2)t}\sqrt{\mu - \kappa^2}\,\mathrm{sech}[\kappa(x - x_0)], \tag{58}$$

which is an example of a dark-bright soliton with

$$\mu_1 = \mu, \quad \mu_2 = \mu - \kappa^2/2. \tag{59}$$

Obviously, $0 < \kappa^2 < \mu$. Assuming $\psi_i(x,t) = e^{-i\mu_i t}\Phi_i(x)$, we can find DB solitons for other values of the parameter g_{12}. Their profiles Φ_i are presented in Fig. 8. They can be intuitively understood as a dip in the probability density of atoms of one kind (species or spin state) and a relatively small peak in the probability density of atoms of the other kind.

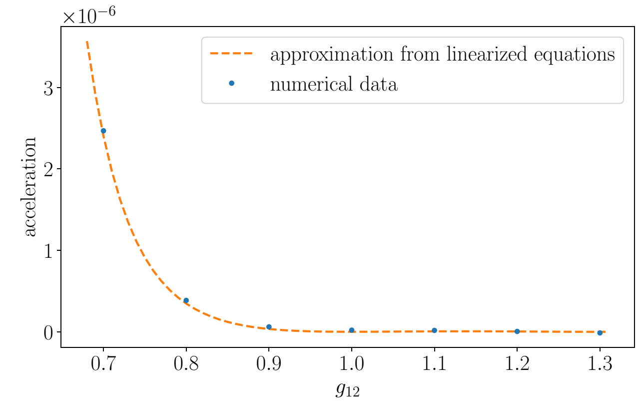

FIG. 10. Acceleration of a dark-bright soliton with $\mu = 1$ and $\kappa = 0.9$ under the influence of the wave in the dark component coming from the left with frequencies $\omega_1^+ = 2.4$ and $\omega_1^- = -0.4$ (i.e., $\tilde{\omega} = -1.4$), $a = 0.05$, and different values of g_{12}.

Consider scattering on such solitons. It can be easily deduced from Eq. (12) that for $x \to \pm\infty$ DB solitons profiles $\Phi_1(x) \to \pm\sqrt{\mu}$, $\Phi_2(x) \to 0$, and $\Phi_i''(x) \to 0$ regardless of the value of g_{12}. Therefore, the matrix $\mathbf{M}$ in Eq. (17) becomes asymptotically

$$\mathbf{M}_{x\to\pm\infty} = \mu\begin{pmatrix} 2 & 1 & 0 & 0 \\ 1 & 2 & 0 & 0 \\ 0 & 0 & g_{12} & 0 \\ 0 & 0 & 0 & g_{12} \end{pmatrix}. \tag{60}$$

Note that this asymptotic form is exactly the same as in the case of scalar dark soliton; therefore, the solutions are the same as in Sec. IV A, in particular the wave number

$$k_1 = \sqrt{2}\sqrt{\sqrt{\mu^2 + \tilde{\omega}^2} - \mu}, \tag{61}$$

and again the waves in the first component propagate for any $\tilde{\omega} \neq 0$. The only difference is that μ_2 is no longer arbitrary

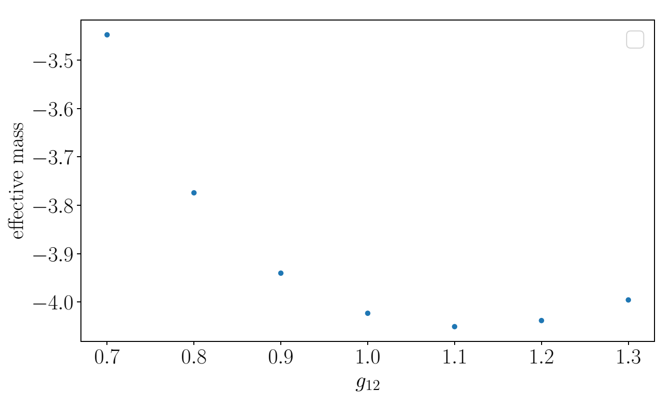

FIG. 9. Effective mass of DB solitons for different values of g_{12}, obtained using solitons at time $t = 60$ after pushing it using the external impulse (70) with the parameters $T = 1$ and $V_0 \in [0.005, 0.08]$. Velocities were obtained using the linear fit to the position of the center of the soliton.

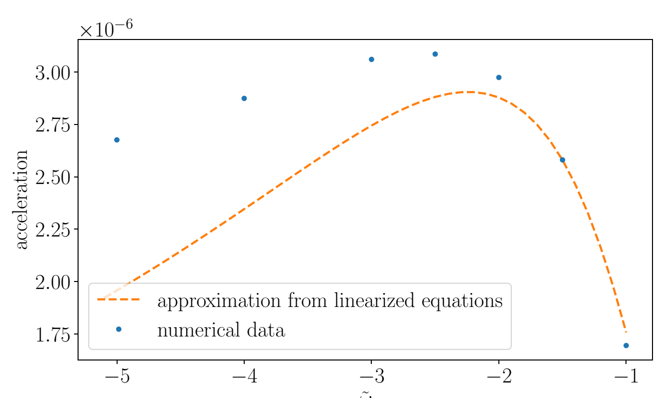

FIG. 11. Acceleration of a dark-bright soliton with $\mu = 1$ and $\kappa = 0.9$ under the influence of the wave in the dark component coming from the left with an amplitude $a = 0.05$, $g_{12} = 0.7$, and different frequencies $\omega_1^\pm = \mu \mp \tilde{\omega}$.

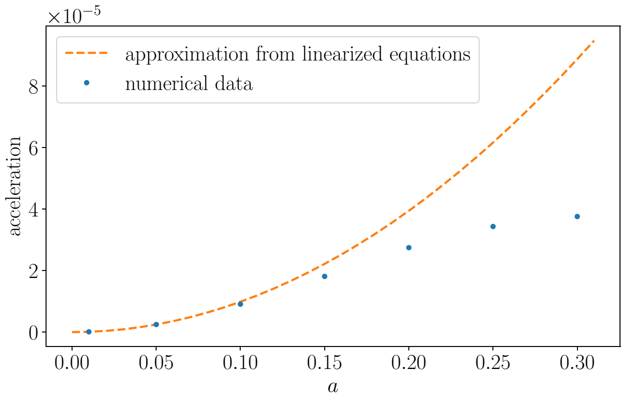

FIG. 12. Acceleration of a dark-bright soliton with $\mu = 1$ and $\kappa = 0.9$ under the influence of the wave in the dark component coming from the left with frequencies $\omega_1^+ = 2.4$ and $\omega_1^- = -0.4$ (i.e., $\tilde{\omega} = -1.4$), $g_{12} = 0.7$, and different amplitudes.

and therefore

$$k_2^{\pm} = \sqrt{2}\sqrt{\mp\tilde{\omega} - \mu g_{12} + \mu - \kappa^2/2}. \qquad (62)$$

Thus, waves in the second component with wave number $k_2^{\pm}$ propagate when $\mp\tilde{\omega} > \mu g_{12} - \mu + \kappa^2/2$. This means that for $\kappa^2 < 2\mu(1 - g_{12})$ there exists a range of $\tilde{\omega}$ in which both waves can propagate with the same $\tilde{\omega}$; however, we were unable to find the stable solitons in this range. For $\kappa^2 \geqslant 2\mu(1 - g_{12})$ with fixed $\tilde{\omega}$ only one (or neither) of the waves can propagate. Note that this excludes the possibility of propagating both types of waves in the second component for $g_{12} \geqslant 1$.

Conditions for moving to the right in the first component are the same as for the scalar dark case. In the second component, they are $\tilde{\omega} < \mu - \kappa^2/2$ for ω_2^+ and $\tilde{\omega} > -\mu + \kappa^2/2$ for ω_2^-. Therefore, for $\tilde{\omega} \in (-\mu + \kappa^2/2, \mu - \kappa^2/2)$ both waves propagate to the right (it is always true because $\mu - \kappa^2/2$ is positive).

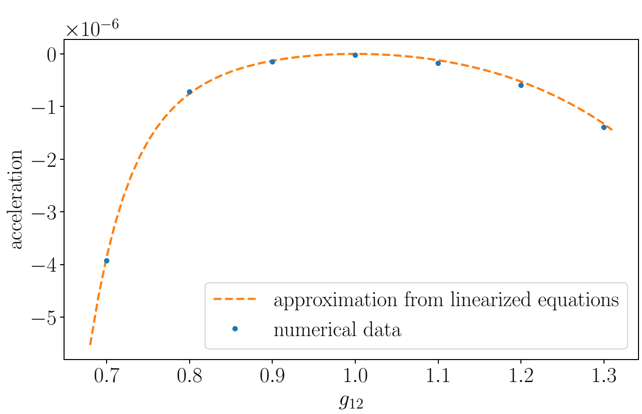

FIG. 13. Acceleration of a dark-bright soliton with $\mu = 1$ and $\kappa = 0.9$ under the influence of the wave in the bright component coming from the left with frequencies $\omega_2^+ = 1.995$ and $\omega_2^- = -0.805$ (i.e., $\tilde{\omega} = -1.4$), $a = 0.05$, and different values of g_{12}.

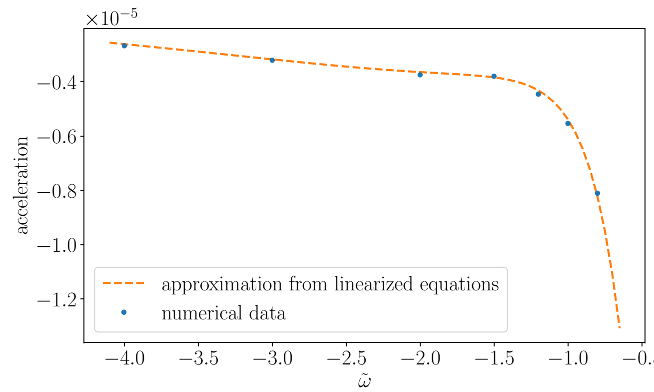

FIG. 14. Acceleration of a dark-bright soliton with $\mu = 1$ and $\kappa = 0.9$ under the influence of the wave in the bright component coming from the left with an amplitude $a = 0.05$, $g_{12} = 0.7$, and different frequencies $\omega_2^+ = \mu - \kappa^2/2 - \tilde{\omega}$.

The moving dark-bright soliton in the Manakov ($g_{12} = 1$) case with velocity v is [23]

$$\psi_1 = e^{-i\mu t}\sqrt{\mu}\{\cos\alpha \tanh[\tilde{\kappa}(x - x_0 - vt)] + i\sin\alpha\},$$

$$\psi_2 = e^{-i[\mu - \tilde{\kappa}^2(1-\tan^2\alpha)/2]t} e^{ivx}\sqrt{(\mu - \kappa^2)\frac{\tilde{\kappa}}{\kappa}}\,\mathrm{sech} \times [\tilde{\kappa}(x - x_0 - vt)], \qquad (63)$$

where

$$\tilde{\kappa} = \frac{\kappa^2 - \mu + \sqrt{2\kappa^2\mu\cos(2\alpha) + \kappa^4 + \mu^2}}{2\kappa}, \qquad (64)$$

$$v = \tilde{\kappa}\tan\alpha. \qquad (65)$$

We compute the renormalized total energy (analogously to the renormalized energy of a dark soliton)

$$E_s = \frac{1}{2}\int_{-\infty}^{\infty}[|\partial_x\psi_1|^2 + |\partial_x\psi_2|^2 + (|\psi_1|^2 - \mu)^2 + |\psi_2|^4 + 2|\psi_1|^2|\psi_2|^2]\mathrm{d}x, \qquad (66)$$

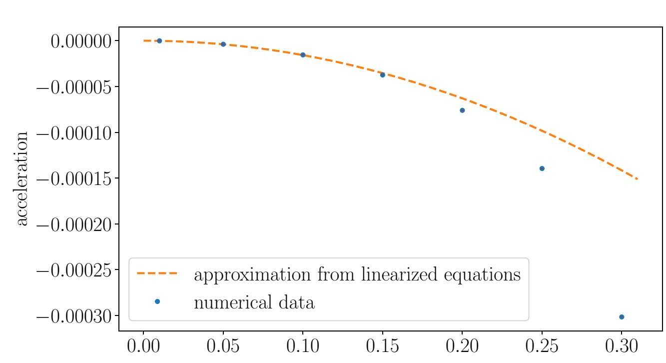

FIG. 15. Acceleration of a dark-bright soliton with $\mu = 1$ and $\kappa = 0.9$ under the influence of the wave in the bright component coming from the left with frequency $\omega_2^+ = 1.995$ (i.e., $\tilde{\omega} = -1.4$), $g_{12} = 0.7$, and different amplitudes.

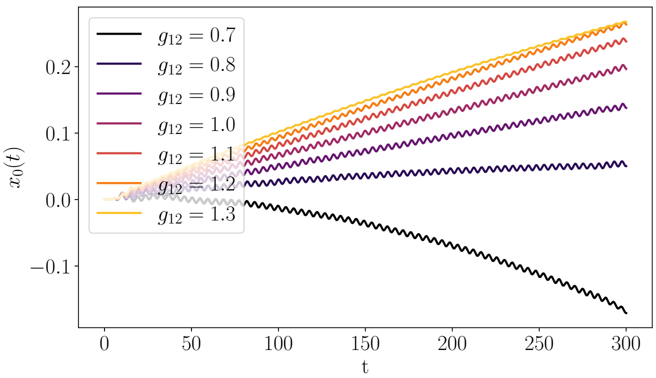

FIG. 16. Position of a dark-bright soliton with $\mu = 1$ and $\kappa = 0.9$ under the influence of the wave in the bright component coming from the left with frequency $\omega_2^+ = 1.995$ (i.e., $\tilde{\omega} = -1.4$), $a = 0.05$, and different values of g_{12}.

and from that we get the effective mass

$$M = \frac{\mathrm{d}^2 E_s}{\mathrm{d}v^2}\bigg|_{v=0} = \left(\frac{\mathrm{d}v}{\mathrm{d}\alpha}\right)^{-2}\left(\frac{\mathrm{d}^2 E_s}{\mathrm{d}\alpha^2} - \frac{\mathrm{d}^2 v}{\mathrm{d}\alpha^2}\frac{\mathrm{d}v}{\mathrm{d}\alpha}\frac{\mathrm{d}E_s}{\mathrm{d}\alpha}\right)\bigg|_{\alpha=0} = -\frac{2(\kappa^2+\mu)}{\kappa}. \quad (67)$$

For $\kappa \to \sqrt{\mu}$ we reproduce the result for the scalar dark soliton $M = -4\sqrt{\mu}$. Using the renormalized total momentum

$$P_s = \frac{i}{2}\int_{-\infty}^{\infty}(\psi_1\partial_x\psi_1^* - \psi_1^*\partial_x\psi_1 + \psi_2\partial_x\psi_2^* - \psi_2^*\partial_x\psi_2)\mathrm{d}x - \mu\Delta\phi, \quad (68)$$

where $\Delta\phi = 2\alpha - \pi$ is the phase change between $-\infty$ and $+\infty$ in the dark (first) component, we obtain the same effective mass

$$M = \frac{\mathrm{d}P_s}{\mathrm{d}v}\bigg|_{v=0} = \left(\frac{\mathrm{d}v}{\mathrm{d}\alpha}\right)^{-1}\frac{\mathrm{d}P_s}{\mathrm{d}\alpha}\bigg|_{\alpha=0} = -\frac{2(\kappa^2+\mu)}{\kappa}. \quad (69)$$

This indicates that the motion of the dark-bright solitons in the Manakov case is indeed Newtonian and that we used the correct renormalization.

In the non-Manakov ($g_{12} \neq 1$) case we push the soliton using the short and localized external impulse

$$V_1(x) = V_0 t(T-t)\theta(t)\theta(T-t)\frac{\tanh(x)}{\cosh(x)}, \quad V_2(x) = 0 \quad (70)$$

and obtain the velocity and moving soliton profile after a sufficiently long time, from which we calculate E_s and compute $M = \frac{d^2E_s}{dv^2}|_{v=0}$ and $M = \frac{dP_s}{dv}|_{v=0}$ by fitting a quadratic function to $E_s(v)$ and a linear function to $P_s(v)$, respectively (Fig. 9). Henceforth, we will use the mass obtained from the momentum, because it is more accurate.

B. Wave in the dark component

Let us consider a DB soliton with a wave in the first component with a wave number k_1 and a small amplitude a coming from the left (provided adequate conditions, discussed in the preceding section, are met). The asymptotics are then

$$\psi_1(x,t) \xrightarrow[x\to-\infty]{} a\beta\left(-\frac{\frac{k_1^2}{2}-\tilde{\omega}}{\mu}-1\right)e^{-i\omega_1^+ t}(e^{ik_1x} + r_1e^{-ik_1x}) + a\beta e^{-i\omega_1^- t}(e^{-ik_1x} + r_1^*e^{ik_1x}) - \sqrt{\mu}e^{-i\mu t},$$

$$\psi_1(x,t) \xrightarrow[x\to+\infty]{} a\beta\left(-\frac{\frac{k_1^2}{2}-\tilde{\omega}}{\mu}-1\right)e^{-i\omega_1^+ t}t_1e^{ik_1x} + a\beta e^{-i\omega_i^- t}t_1^*e^{-ik_1x} + \sqrt{\mu}e^{-i\mu t},$$

$$\psi_2(x,t) \xrightarrow[x\to-\infty]{} ae^{-i\omega_2^+ t}r_2^+e^{-ik_2^+x} + ae^{-i\omega_2^- t}r_2^-e^{-ik_2^-x},$$

$$\psi_2(x,t) \xrightarrow[x\to+\infty]{} ae^{-i\omega_2^+ t}t_2^+e^{ik_2^+x} + ae^{-i\omega_2^- t}t_2^-e^{ik_2^-x}, \quad (71)$$

where β is the same as in Eq. (50). Using an analogous approach as before, we derive that the force exerted on the soliton by such a wave is

$$F = a^2\big[k_1^2(1+R_1-T_1) + (k_2^+)^2(R_2^+ - T_2^+) + (k_2^-)^2(R_2^- - T_2^-)\big], \quad (72)$$

where $R_1 = |r_1|^2$, $T_1 = |t_1|^2$, $R_2^\pm = |r_2^\pm|^2$, and $T_2^\pm = |t_2^\pm|^2$.

The setup (71) corresponds to the eigenwave (25) with $A = 0$; let us call it the first eigenwave. The other eigenwave ($B = 0$), i.e., Eq. (71) with $k_1 \to -k_1$, gives the same expression for the effective force, but with different values of reflection and transmission coefficients. Let us focus on the first eigenwave (note that the conditions for propagation to the right are derived above for the first eigenwave). Using an approach similar to that for the scalar soliton, we can compute values of these coefficients and (using the effective mass computed above) compare the resulting acceleration with full PDE simulations (with initial field configurations constructed analogously as for the scalar dark soliton). It turns out that we always get the negative radiation pressure, described well by our linear model for relatively small amplitudes and frequencies (Figs. 10–12). The nonlinear behavior for larger amplitudes is expected, since linear approach relies on the fact that the amplitude is small. However, the discrepancy for larger frequencies is surprising and requires further study.

C. Wave in the bright component

If we consider a DB soliton with a wave in the second component with a wave number $k_2^\pm$ (and a small amplitude a) coming from the left, the asymptotics are

$$\psi_1(x,t) \xrightarrow[x\to-\infty]{} a\beta\left(-\frac{\frac{k_1^2}{2}-\tilde{\omega}}{\mu}-1\right)e^{-i\omega_1^+ t}r_1e^{-ik_1x} + a\beta e^{-i\omega_1^- t}r_1^*e^{ik_1x} - \sqrt{\mu}e^{-i\mu t},$$

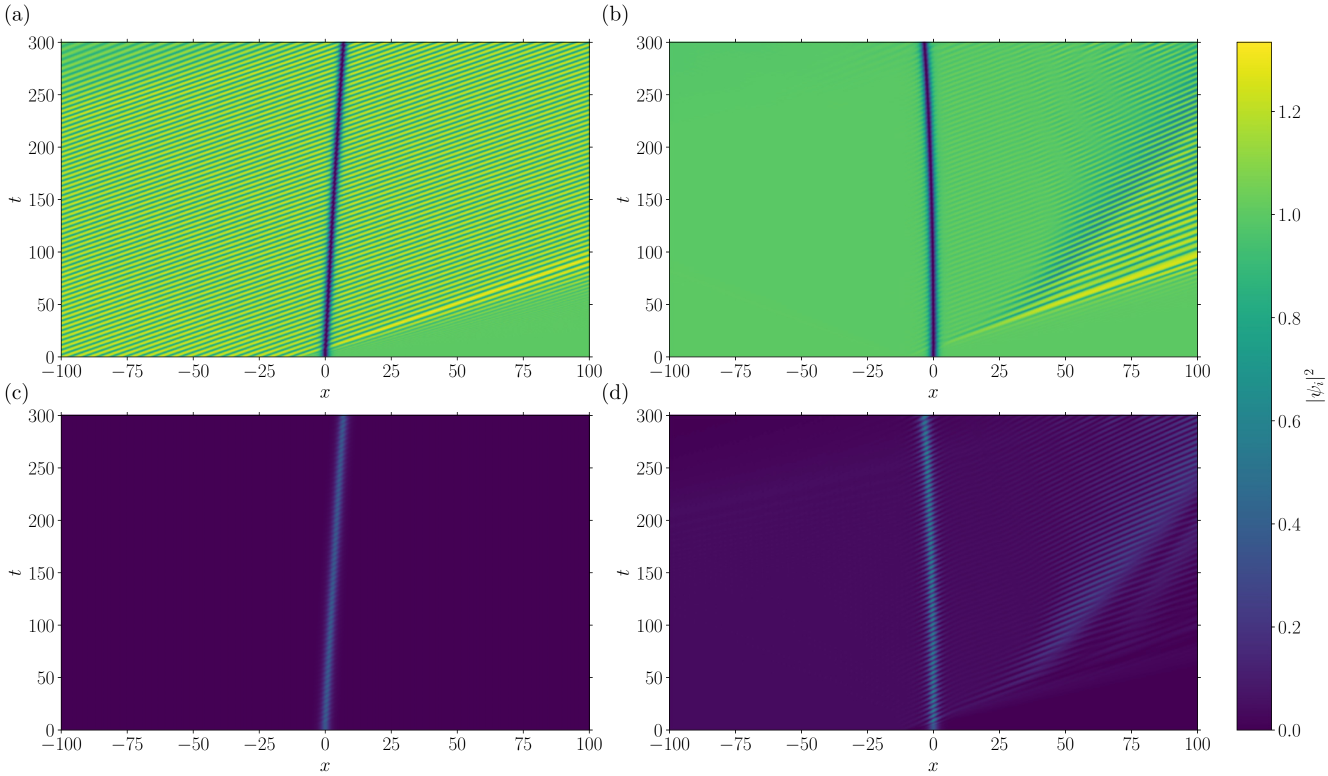

FIG. 17. Evolution of the dark-bright soliton with $\mu = 1$, $\kappa = 0.9$, and $g_{12} = 0.7$, interacting with a wave in the (a) and (c) dark and (b) and (d) bright component coming from the left with frequencies corresponding to $\tilde{\omega} = -1.4$ and amplitude $a = 0.2$. The probability densities of [(a) and (b)] the dark and [(c) and (d)] the bright components are presented.

$$\begin{aligned}
\psi_1(x,t) &\xrightarrow[x\to+\infty]{} a\beta\left(-\frac{\frac{k_1^2}{2}-\tilde{\omega}}{\mu}-1\right)e^{-i\omega_1^+ t}t_1 e^{ik_1x} + a\beta e^{-i\omega_i^- t}t_1^* e^{-ik_1x} + \sqrt{\mu}e^{-i\mu t},\\
\psi_2(x,t) &\xrightarrow[x\to-\infty]{} ae^{-i\omega_2^\pm t}e^{ik_2^\pm x} + ae^{-i\omega_2^+ t}r_2^+ e^{-ik_2^+ x} + ae^{-i\omega_2^- t}r_2^- e^{-ik_2^- x},\\
\psi_2(x,t) &\xrightarrow[x\to+\infty]{} ae^{-i\omega_2^+ t}t_2^+ e^{ik_2^+ x} + ae^{-i\omega_2^- t}t_2^- e^{ik_2^- x},
\end{aligned} \tag{73}$$

with β the same as in Eq. (50). Similarly to before, we can derive the force exerted on the soliton

$$\begin{aligned}
F = {}& a^2\big[k_1^2(R_1 - T_1) + (k_2^+)^2(R_2^+ - T_2^+) + (k_2^-)^2(R_2^- - T_2^-)\\
&+ (k_2^\pm)^2\big],
\end{aligned} \tag{74}$$

where $R_1 = |r_1|^2$, $T_1 = |t_1|^2$, $R_2^\pm = |r_2^\pm|^2$, and $T_2^\pm = |t_2^\pm|^2$.

Again, we compute the values of the reflection and transmission coefficients numerically and compare the resulting acceleration with the full PDE simulations. In this case we observe the positive radiation pressure for all the values of parameters considered, and everything is described well by the linearized model provided the amplitude is small (Figs. 13–16). Examples of the evolution for waves in the both components are presented in Fig. 17.

D. Dark-bright solitons in a harmonic trap

To verify how well the above results apply in realistic situations, let us include a harmonic trapping potential

$$V_1(x) = V_2(x) = \tfrac{1}{2}\omega_x^2 x^2 \tag{75}$$

in Eq. (3), solve it numerically, and compare with the linearized approximations obtained without a trap. In this section we use physical units, unless we specifically refer to our units, defined in Sec. II A. In order for the parameters to be possible to achieve in experiments, we choose the trapping frequencies used in [36], i.e., $\omega_x = 2\pi \times 14$ Hz and $\omega_\perp = 2\pi \times 425$ Hz. Similarly, we normalize ψ_i to the numbers of atoms $N_1 \approx 152\,500$ and $N_2 \approx 1700$ in the dark and bright components, respectively. Again, N_1 was inspired by [36], while the proportion $N_2 \approx 0.01N_1$ is similar to that in [33]. We choose $a_{11} = a_{22} \approx 100a_0$ and $a_{12} \approx 110a_0$, where a_0 is the Bohr radius. With these parameters, we use the gradient flow method and find a dark-bright soliton, presented in Fig. 18.

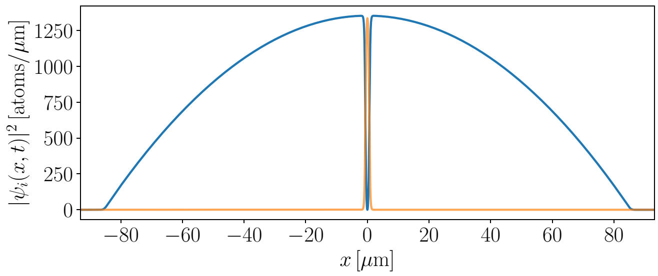

FIG. 18. Dark-bright soliton in a harmonic trap with a frequency $\omega_x = 2\pi \times 14$ Hz and $\omega_\perp = 2\pi \times 425$ Hz in a CNLSE with $a_{12} \approx 110a_0$ (in our units $g_{12} = 1.1$). The numbers of atoms are about $N_1 \approx 152\,500$ and $N_2 \approx 1700$ in the dark [blue (darker) line] and bright [orange (lighter) line] components, respectively, which correspond to $\mu = 35\,000$ and $\kappa = 20$ in our units.

We simulated collisions of the DB soliton with monochromatic waves of several frequencies, incoming from both the dark and the bright component. The amplitudes of these waves were equal to about 10% of the amplitude of the DB soliton's dark component, corresponding to $a = 20$ in our units. Despite the fact that the linearized approximation does not include a trap, the measured accelerations followed somewhat similar curves (Fig. 19). The accelerations were measured only in the short time interval (about first 4 ms), since for longer times the force gets affected more by the harmonic potential (see an example of trajectories in Fig. 20).

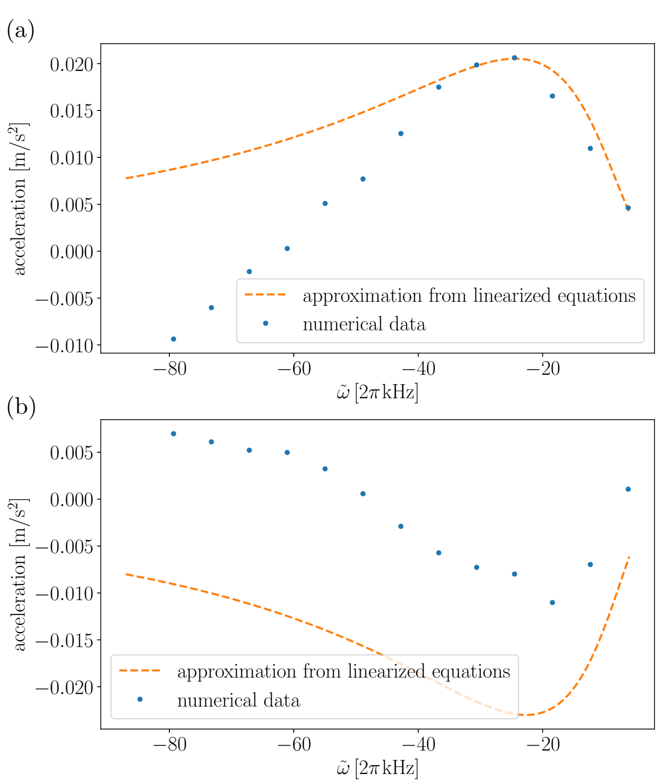

FIG. 19. Acceleration of the dark-bright soliton (Fig. 18) in a harmonic trap under the influence of waves in the (a) dark and (b) bright components, coming from the left with different frequencies and amplitude $a \approx 0.1\sqrt{\mu}$, compared with a linear approximation without a trapping potential.

VI. CONCLUSION

Using the Newtonian approximation and staying in the linear regime, we have successfully described the acceleration of the scatterer due to the action of the radiation pressure of a wave scattering on a dark and a dark-bright soliton. This simple model agrees with numerical simulations for a wide range of parameters. We have shown that a collision of a scalar dark soliton with a wave in the second component of the condensate always results in a positive radiation pressure. For dark-bright solitons, however, we found that the radiation pressure is negative if the wave is incoming from the dark component and positive otherwise. Our results provide a quantitative description for idealized homogenous BECs and a qualitative model for more realistic trapped condensates.

The mechanism responsible for NRP in this model relies on the fact that the soliton is present in both components. Otherwise, the equations separate, and from the conservation of energy it follows that the reflection and transmission coefficients sum to one. This implies that the force is always non-negative, as we have seen explicitly for the scalar soliton case. If the soliton is a vector soliton, then the constraints from the energy conservation allow for both positive and negative signs of the force. Furthermore, the dispersion relations (i.e., the wave numbers k_1 and $k_2^{\pm}$) play an important role in determining this sign (see Table I).

The discrepancies between our effective linear model and the full PDE simulations are completely expected for the larger amplitudes of the incoming wave, since the linearization relies on it being small. However, the disagreement for large frequencies of the wave incoming from the dark component and hitting the dark-bright soliton is currently not well understood within the scope of this paper. This could be an opportunity for further research, especially combined with a detailed study of the nonlinear effects, which can play a role here. Another interesting possibility would be to investigate NRP on other solitons in a two-component BEC, such as bright-bright and dark-dark solitons.

It is also worth mentioning that there is a correspondence between dark (dark-bright) solitons and Néel (Bloch) walls in the parametrically driven nonlinear Schrödinger equation [75–82], although with different dynamics. Moreover, the problem described in this paper shows some similarities to the wall-on-wall scattering described in [82], which is an interesting topic for further study.

The described setups can in principle be reproduced experimentally. Hopefully, in the future, this article could help to promote NRP from being a purely theoretical concept to an observable physical phenomenon.

ACKNOWLEDGMENTS

T.R. acknowledges the support of Polish National Science Centre, Grant No. NCN 2019/35/B/ST2/00059. D.C. and T.R. are grateful for support from the Priority Research Area under the program Excellence Initiative of Research University at the Jagiellonian University in Kraków. The authors would

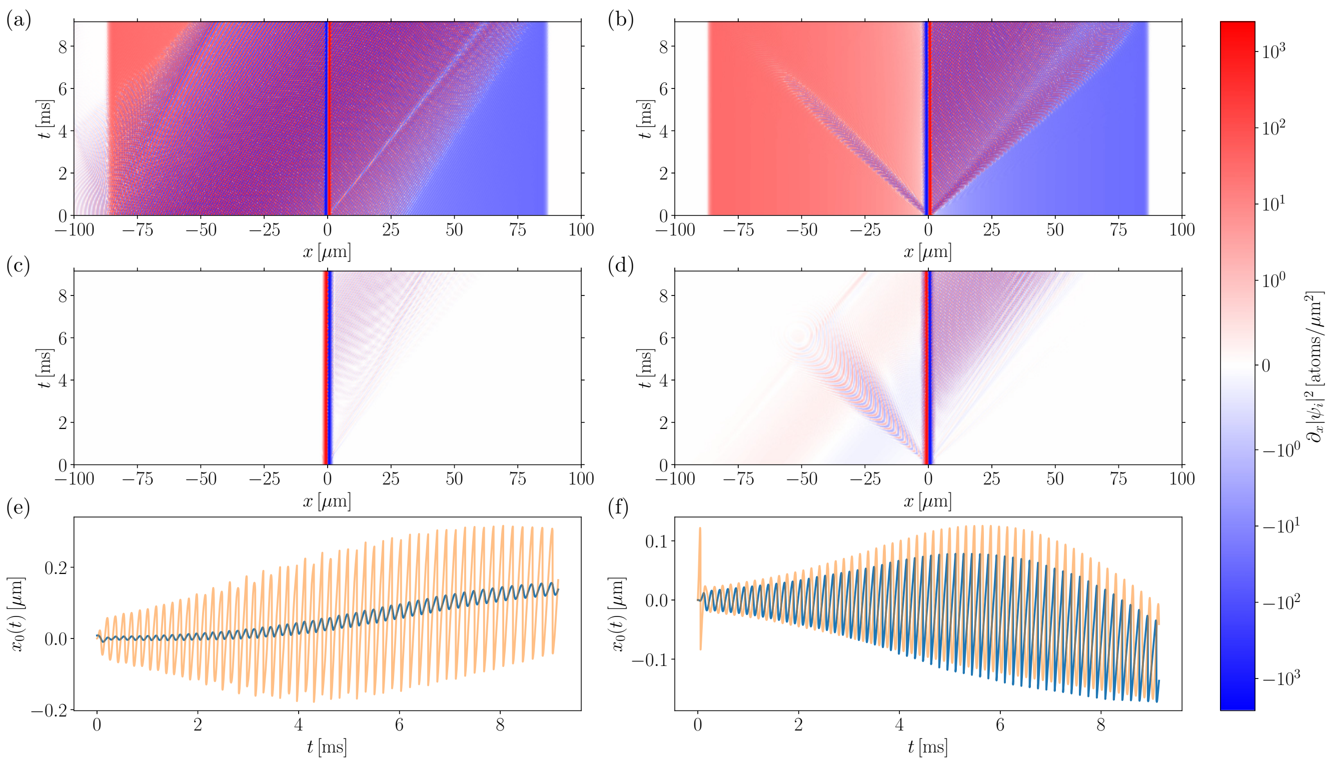

FIG. 20. Evolution of the dark-bright soliton in a harmonic trap (Fig. 18), interacting with a wave in the [(a), (c), and (e)] dark and [(b), (d), and (f)] bright components coming from the left with frequencies $\omega_1^+ = 2\pi \times 12\,351$ Hz, $\omega_1^- = -2\pi \times 174$ Hz, and $\omega_2^+ = 2\pi \times 12\,386$ Hz (i.e., $\tilde{\omega} = -2\pi \times 6263$ Hz) and amplitude $a \approx 0.1\sqrt{\mu}$. Spatial derivatives of the probability density of [(a) and (b)] the dark and [(c) and (d)] the bright components are presented as functions of time and space. (e) and (f) Additionally, the positions of the dark [blue (darker) line] and bright [orange (lighter) line] parts of the soliton are shown as functions of time.

like to express their gratitude to Adam Wojciechowski and Krzysztof Sacha for useful discussions, especially on the experimental applications of this research.

APPENDIX A: DERIVATION OF TOTAL ENERGY AND MOMENTUM

Using the Lagrangian density (4), we can derive the energy-momentum tensor

$$T^\mu_\nu = \sum_{i=1,2}\left(\frac{\partial\mathcal{L}}{\partial(\partial_\mu\psi_i)}\partial_\nu\psi_i + \frac{\partial\mathcal{L}}{\partial(\partial_\mu\psi_i^*)}\partial_\nu\psi_i^*\right) - \mathcal{L}\delta^\mu_\nu, \quad \text{(A1)}$$

where $\mu, \nu = 0, 1$; $\partial_0 = \partial_t$; and $\partial_1 = \partial_x$. Since we consider CNLSEs without the trapping potential, the Lagrangian density (4) is invariant under translations, and then from the Noether theorem it follows that such a tensor is a conserved current, meaning that it obeys

$$\sum_{\mu=1,2}\partial_\mu T^\mu_\nu = 0. \quad \text{(A2)}$$

The total energy and momentum are defined

$$E = \int_{-\infty}^{\infty} T^0_0 \mathrm{d}x, \quad P = -\int_{-\infty}^{\infty} T^0_1 \mathrm{d}x, \quad \text{(A3)}$$

respectively. Computing the energy-momentum tensor and integrating, we obtain their explicit form (5) and (6). Then Eqs. (7) and (8) follow from (A2).

APPENDIX B: NUMERICAL METHODS

In all of the simulations of soliton dynamics in the full PDE, we have used the second-order split-step method [83].

TABLE I. Example of reflection and transmission coefficients (derived from linearized equations) and the formulas present in the effective forces (72) and (74). Kronecker deltas are such that we set $i = 1$ for the wave incoming from the dark component and $i = 2$ for the bright. The parameters of the soliton and the scattered wave are $\mu = 1$, $\kappa = 0.9$, $g_{12} = 0.7$, and $\tilde{\omega} = -1.4$. Note that the wave numbers change the sign of the total force.

Coefficient	Wave from dark	Wave from bright
R_1	1.511×10^{-6}	4.792×10^{-6}
T_1	9.930×10^{-1}	9.325×10^{-3}
R_2^+	2.666×10^{-6}	1.601×10^{-4}
T_2^+	5.188×10^{-3}	9.929×10^{-1}
$\delta_{i1} + R_1 - T_1$	6.962×10^{-3}	-9.321×10^{-3}
$\delta_{i2} + R_2^+ - T_2^+$	-5.185×10^{-3}	7.279×10^{-3}
$k_1^2(\delta_{i1} + R_1 - T_1)$	1.003×10^{-2}	-1.343×10^{-2}
$(k_2^+)^2(\delta_{i2} + R_2^+ - T_2^+)$	-1.343×10^{-2}	1.885×10^{-2}

This method requires periodic boundary conditions; therefore, at large x the dark soliton (and the dark part of the dark bright soliton) was glued to the antisoliton to achieve $\psi_1 = -\sqrt{\mu}$ at the right boundary. The spatial step was $\Delta x = 0.1$, while the temporal step was in the range from $\Delta t = 0.0001$ to $\Delta t = 0.0003$, depending on a particular simulated configuration. We used $x \in [-500, 1000]$ or $x \in [-1000, 2000]$. Other methods with other boundary conditions are possible to implement in CNLSEs (see, e.g., [84]).

Linearized equations were solved using sparse matrices. The derivatives were discretized using the five-point stencil. The grid was $x \in [-20, 20]$ with the step $\Delta x = 0.01$. The size of the grid in this problem does not need to match the size of the spatial grid used in solving the full PDE. In fact, we verified that the solutions to linearized equations do not depend on the grid size, provided it is sufficiently large, such that the solutions achieve the expected asymptotic form.

[1] G. P. Agrawal and Y. S. Kivshar, *Optical Solitons* (Elsevier, Amsterdam, 2003).

[2] M. H. Anderson, J. R. Ensher, M. R. Matthews, C. E. Wieman, and E. A. Cornell, Observation of Bose-Einstein condensation in a dilute atomic vapor, Science **269**, 198 (1995).

[3] R. Carretero-González, D. J. Frantzeskakis, and P. G. Kevrekidis, Nonlinear waves in Bose–Einstein condensates: Physical relevance and mathematical techniques, Nonlinearity **21**, R139 (2008).

[4] E. G. Charalampidis, P. G. Kevrekidis, D. J. Frantzeskakis, and B. A. Malomed, Dark-bright solitons in coupled nonlinear Schrödinger equations with unequal dispersion coefficients, Phys. Rev. E **91**, 012924 (2015).

[5] B. Deconinck, J. N. Kutz, M. S. Patterson, and B. W. Warner, Dynamics of periodic multi-component Bose–Einstein condensates, J. Phys. A: Math. Gen. **36**, 5431 (2003).

[6] G. Modugno, M. Modugno, F. Riboli, G. Roati, and M. Inguscio, Two atomic species superfluid, Phys. Rev. Lett. **89**, 190404 (2002).

[7] D. S. Hall, M. R. Matthews, J. R. Ensher, C. E. Wieman, and E. A. Cornell, Dynamics of component separation in a binary mixture of Bose-Einstein condensates, Phys. Rev. Lett. **81**, 1539 (1998).

[8] F. Baronio, A. Degasperis, M. Conforti, and S. Wabnitz, Solutions of the vector nonlinear Schrödinger equations: Evidence for deterministic rogue waves, Phys. Rev. Lett. **109**, 044102 (2012).

[9] A. Degasperis, M. Conforti, F. Baronio, and S. Wabnitz, Effects of nonlinear wave coupling: Accelerated solitons, Eur. Phys. J.: Spec. Top. **147**, 233 (2007).

[10] T. Tsuzuki, Nonlinear waves in the Pitaevskii-Gross equation, J. Low Temp. Phys. **4**, 441 (1971).

[11] A. Hasegawa and F. Tappert, Transmission of stationary nonlinear optical pulses in dispersive dielectric fibers. II. Normal dispersion, Appl. Phys. Lett. **23**, 171 (1973).

[12] K. Blow and N. Doran, Multiple dark soliton solutions of the nonlinear Schrödinger equation, Phys. Lett. A **107**, 55 (1985).

[13] V. E. Zakharov and A. B. Shabat, Interaction between solitons in a stable medium, Zh. Eksp. Teor. Fiz. **64**, 1627 (1973) [Sov. Phys. JETP **37**, 823 (1973)].

[14] L. Lerner, D. J. Mitchell, and A. W. Snyder, Interacting gray solitons, Opt. Lett. **19**, 1302 (1994).

[15] L. Gagnon, Solitons on a continuous-wave background and collision between two dark pulses: Some analytical results, J. Opt. Soc. Am. B **10**, 469 (1993).

[16] R. N. Thurston and A. M. Weiner, Collisions of dark solitons in optical fibers, J. Opt. Soc. Am. B **8**, 471 (1991).

[17] Y. S. Kivshar and X. Yang, Perturbation-induced dynamics of dark solitons, Phys. Rev. E **49**, 1657 (1994).

[18] V. V. Konotop and V. E. Vekslerchik, Direct perturbation theory for dark solitons, Phys. Rev. E **49**, 2397 (1994).

[19] X.-J. Chen, Z.-D. Chen, and N.-N. Huang, A direct perturbation theory for dark solitons based on a complete set of the squared Jost solutions, J. Phys. A: Math. Gen. **31**, 6929 (1998).

[20] N.-N. Huang, S. Chi, and X.-J. Chen, Foundation of direct perturbation method for dark solitons, J. Phys. A: Math. Gen. **32**, 3939 (1999).

[21] V. M. Lashkin, Perturbation theory for dark solitons: Inverse scattering transform approach and radiative effects, Phys. Rev. E **70**, 066620 (2004).

[22] I. M. Uzunov and V. S. Gerdjikov, Self-frequency shift of dark solitons in optical fibers, Phys. Rev. A **47**, 1582 (1993).

[23] T. Busch and J. R. Anglin, Dark-bright solitons in inhomogeneous Bose-Einstein condensates, Phys. Rev. Lett. **87**, 010401 (2001).

[24] M. Vijayajayanthi, T. Kanna, and M. Lakshmanan, Bright-dark solitons and their collisions in mixed N-coupled nonlinear Schrödinger equations, Phys. Rev. A **77**, 013820 (2008).

[25] S. Rajendran, P. Muruganandam, and M. Lakshmanan, Interaction of dark–bright solitons in two-component Bose–Einstein condensates, J. Phys. B **42**, 145307 (2009).

[26] V. A. Brazhnyi and V. M. Pérez-García, Stable multidimensional soliton stripes in two-component Bose–Einstein condensates, Chaos Soliton. Fract. **44**, 381 (2011).

[27] C. Yin, N. G. Berloff, V. M. Pérez-García, D. Novoa, A. V. Carpentier, and H. Michinel, Coherent atomic soliton molecules for matter-wave switching, Phys. Rev. A **83**, 051605(R) (2011).

[28] K. J. H. Law, P. G. Kevrekidis, and L. S. Tuckerman, Stable vortex–bright-soliton structures in two-component Bose-Einstein condensates, Phys. Rev. Lett. **105**, 160405 (2010).

[29] V. Achilleos, P. G. Kevrekidis, V. M. Rothos, and D. J. Frantzeskakis, Statics and dynamics of atomic dark-bright solitons in the presence of impurities, Phys. Rev. A **84**, 053626 (2011).

[30] A. Álvarez, J. Cuevas, F. Romero, and P. Kevrekidis, Dark–bright discrete solitons: A numerical study of existence, stability and dynamics, Physica D **240**, 767 (2011).

[31] H. E. Nistazakis, D. J. Frantzeskakis, P. G. Kevrekidis, B. A. Malomed, and R. Carretero-González, Bright-dark soliton complexes in spinor Bose-Einstein condensates, Phys. Rev. A **77**, 033612 (2008).

[32] C. Becker, S. Stellmer, P. Soltan-Panahi, S. Dörscher, M. Baumert, E.-M. Richter, J. Kronjäger, K. Bongs, and K. Sengstock, Oscillations and interactions of dark and dark–

bright solitons in Bose–Einstein condensates, Nat. Phys. **4**, 496 (2008).

[33] S. Middelkamp, J. Chang, C. Hamner, R. Carretero-González, P. Kevrekidis, V. Achilleos, D. Frantzeskakis, P. Schmelcher, and P. Engels, Dynamics of dark–bright solitons in cigar-shaped Bose–Einstein condensates, Phys. Lett. A **375**, 642 (2011).

[34] C. Hamner, J. J. Chang, P. Engels, and M. A. Hoefer, Generation of dark-bright soliton trains in superfluid-superfluid counterflow, Phys. Rev. Lett. **106**, 065302 (2011).

[35] D. Yan, J. J. Chang, C. Hamner, P. G. Kevrekidis, P. Engels, V. Achilleos, D. J. Frantzeskakis, R. Carretero-González, and P. Schmelcher, Multiple dark-bright solitons in atomic Bose-Einstein condensates, Phys. Rev. A **84**, 053630 (2011).

[36] S. Burger, K. Bongs, S. Dettmer, W. Ertmer, K. Sengstock, A. Sanpera, G. V. Shlyapnikov, and M. Lewenstein, Dark solitons in Bose-Einstein condensates, Phys. Rev. Lett. **83**, 5198 (1999).

[37] J. Denschlag, J. E. Simsarian, D. L. Feder, C. W. Clark, L. A. Collins, J. Cubizolles, L. Deng, E. W. Hagley, K. Helmerson, W. P. Reinhardt, S. L. Rolston, B. I. Schneider, and W. D. Phillips, Generating solitons by phase engineering of a Bose-Einstein condensate, Science **287**, 97 (2000).

[38] Z. Dutton, M. Budde, C. Slowe, and L. V. Hau, Observation of quantum shock waves created with ultra-compressed slow light pulses in a Bose-Einstein condensate, Science **293**, 663 (2001).

[39] B. P. Anderson, P. C. Haljan, C. A. Regal, D. L. Feder, L. A. Collins, C. W. Clark, and E. A. Cornell, Watching dark solitons decay into vortex rings in a Bose-Einstein condensate, Phys. Rev. Lett. **86**, 2926 (2001).

[40] K. Bongs, S. Burger, S. Dettmer, D. Hellweg, J. Arlt, W. Ertmer, and K. Sengstock, Coherent manipulation and guiding of Bose–Einstein condensates by optical dipole potentials, C. R. Acad. Sci. IV—Phys. **2**, 671 (2001).

[41] Z. Chen, M. Segev, T. H. Coskun, D. N. Christodoulides, Y. S. Kivshar, and V. V. Afanasjev, Incoherently coupled dark–bright photorefractive solitons, Opt. Lett. **21**, 1821 (1996).

[42] Z. Chen, M. Segev, T. H. Coskun, D. N. Christodoulides, and Y. S. Kivshar, Coupled photorefractive spatial-soliton pairs, J. Opt. Soc. Am. B **14**, 3066 (1997).

[43] D. Foursa and P. Emplit, Investigation of black-gray soliton interaction, Phys. Rev. Lett. **77**, 4011 (1996).

[44] D. J. Frantzeskakis, Dark solitons in atomic Bose–Einstein condensates: From theory to experiments, J. Phys. A: Math. Theor. **43**, 213001 (2010).

[45] P. Kevrekidis and D. Frantzeskakis, Solitons in coupled nonlinear Schrödinger models: A survey of recent developments, Rev. Phys. **1**, 140 (2016).

[46] *Emergent Nonlinear Phenomena in Bose-Einstein Condensates: Theory and Experiment*, edited by P. G. Kevrekidis, D. J. Frantzeskakis, and R. Carretero-González, Springer Series on Atomic, Optical and Plasma Physics Vol. 45 (Springer, Berlin, 2008).

[47] L. Pitaevskii and S. Stringari, *Bose-Einstein Condensation* (Clarendon Press, Oxford, 2003).

[48] S. V. Manakov, On the theory of two-dimensional stationary self-focusing of electromagnetic waves, Zh. Eksp. Teor. Fiz. **65**, 505 (1973) [Sov. Phys. JETP **38**, 248 (1974)].

[49] H. Shin, Soliton on a cnoidal wave background in the coupled nonlinear Schrödinger equation, J. Phys. A: Math. Gen. **37**, 8017 (2004).

[50] P. Forgács, A. Lukács, and T. Romańczukiewicz, Plane waves as tractor beams, Phys. Rev. D **88**, 125007 (2013).

[51] D. Yan, J. J. Chang, C. Hamner, M. Hoefer, P. G. Kevrekidis, P. Engels, V. Achilleos, D. J. Frantzeskakis, and J. Cuevas, Beating dark–dark solitons in Bose–Einstein condensates, J. Phys. B **45**, 115301 (2012).

[52] L. D. Carr, M. A. Leung, and W. P. Reinhardt, Dynamics of the Bose-Einstein condensate: Quasi-one-dimension and beyond, J. Phys. B **33**, 3983 (2000).

[53] G. C. Katsimiga, J. Stockhofe, P. G. Kevrekidis, and P. Schmelcher, Stability and dynamics of dark-bright soliton bound states away from the integrable limit, Appl. Sci. **7**, 388 (2017).

[54] C. Chin, R. Grimm, P. Julienne, and E. Tiesinga, Feshbach resonances in ultracold gases, Rev. Mod. Phys. **82**, 1225 (2010).

[55] A. Burchianti, C. D'Errico, M. Prevedelli, L. Salasnich, F. Ancilotto, M. Modugno, F. Minardi, and C. Fort, A dual-species Bose-Einstein condensate with attractive interspecies interactions, Condens. Matter **5**, 21 (2020).

[56] G. Thalhammer, G. Barontini, L. De Sarlo, J. Catani, F. Minardi, and M. Inguscio, Double species Bose-Einstein condensate with tunable interspecies interactions, Phys. Rev. Lett. **100**, 210402 (2008).

[57] S. Tojo, Y. Taguchi, Y. Masuyama, T. Hayashi, H. Saito, and T. Hirano, Controlling phase separation of binary Bose-Einstein condensates via mixed-spin-channel Feshbach resonance, Phys. Rev. A **82**, 033609 (2010).

[58] D.-S. Wang, D.-J. Zhang, and J. Yang, Integrable properties of the general coupled nonlinear Schrödinger equations, J. Math. Phys. **51**, 023510 (2010).

[59] T. Romanczukiewicz, Interaction between kink and radiation in ϕ^4 model, Acta Phys. Pol. B **35**, 523 (2004).

[60] T. Romanczukiewicz, Negative radiation pressure in the case of two interacting fields, Acta Phys. Pol. B **39**, 3449 (2008).

[61] P. Forgács, A. Lukács, and T. Romańczukiewicz, Negative radiation pressure exerted on kinks, Phys. Rev. D **77**, 125012 (2008).

[62] P. Dorey, K. Mersh, T. Romanczukiewicz, and Y. Shnir, Kink-antikink collisions in the ϕ^6 model, Phys. Rev. Lett. **107**, 091602 (2011).

[63] T. Romańczukiewicz, Could the primordial radiation be responsible for vanishing of topological defects?, Phys. Lett. B **773**, 295 (2017).

[64] L. E. Young-S., L. Salasnich, and S. K. Adhikari, Dimensional reduction of a binary Bose-Einstein condensate in mixed dimensions, Phys. Rev. A **82**, 053601 (2010).

[65] M. Trippenbach, K. Góral, K. Rzazewski, B. Malomed, and Y. B. Band, Structure of binary Bose-Einstein condensates, J. Phys. B **33**, 4017 (2000).

[66] H. Tran, Stability of dark solitons: Linear analysis, Phys. Rev. A **46**, 7319 (1992).

[67] P. B. Walczak and J. R. Anglin, Exact Bogoliubov–de Gennes solutions for gray-soliton backgrounds, Phys. Rev. A **84**, 013611 (2011).

[68] D. E. Pelinovsky and M. Plum, Stability of black solitons in optical systems with intensity-dependent dispersion, arXiv:2205.10177.

[69] T. Busch and J. R. Anglin, Motion of dark solitons in trapped Bose-Einstein condensates, Phys. Rev. Lett. **84**, 2298 (2000).

[70] I. V. Barashenkov and E. Y. Panova, Stability and evolution of the quiescent and travelling solitonic bubbles, Physica D **69**, 114 (1993).

[71] D. Kovrizhin, Exact form of the Bogoliubov excitations in one-dimensional nonlinear Schrödinger equation, Phys. Lett. A **287**, 392 (2001).

[72] E. Kuznetsov and S. Turitsyn, Instability and collapse of solitons in media with a defocusing nonlinearity, Zh. Eksp. Teor. Fiz. **94**, 119 (1988) [Sov. Phys. JETP **67**, 1583 (1988).

[73] G. Huang and N. Compagnon, Complete and orthonormal eigenfunctions of excitations to a one-dimensional dark soliton, Phys. Lett. A **372**, 321 (2008).

[74] M. J. Quist, Vortex dynamics in the nonlinear Schrödinger equation, Phys. Rev. B **60**, 4240 (1999).

[75] R. Rajaraman and E. J. Weinberg, Internal symmetry and the semiclassical method in quantum field theory, Phys. Rev. D **11**, 2950 (1975).

[76] S. Sarker, S. Trullinger, and A. Bishop, Solitary-wave solution for a complex one-dimensional field, Phys. Lett. A **59**, 255 (1976).

[77] C. Elphick and E. Meron, Localized structures in surface waves, Phys. Rev. A **40**, 3226 (1989).

[78] P. Coullet, J. Lega, B. Houchmandzadeh, and J. Lajzerowicz, Breaking chirality in nonequilibrium systems, Phys. Rev. Lett. **65**, 1352 (1990).

[79] D. V. Skryabin, A. Yulin, D. Michaelis, W. J. Firth, G.-L. Oppo, U. Peschel, and F. Lederer, Perturbation theory for domain walls in the parametric Ginzburg-Landau equation, Phys. Rev. E **64**, 056618 (2001).

[80] I. V. Barashenkov and S. R. Woodford, Complexes of stationary domain walls in the resonantly forced Ginsburg-Landau equation, Phys. Rev. E **71**, 026613 (2005).

[81] I. V. Barashenkov, S. R. Woodford, and E. V. Zemlyanaya, Interactions of parametrically driven dark solitons. I. Néel-Néel and Bloch-Bloch interactions, Phys. Rev. E **75**, 026604 (2007).

[82] I. V. Barashenkov and S. R. Woodford, Interactions of parametrically driven dark solitons. II. Néel-Bloch interactions, Phys. Rev. E **75**, 026605 (2007).

[83] G. M. Muslu and H. A. Erbay, in *Numerical Mathematics and Advanced Applications*, edited by M. Feistauer, V. Dolejší, P. Knobloch, and K. Najzar (Springer, Berlin, 2004), pp. 658–667.

[84] R. M. Caplan and R. Carretero-González, A modulus-squared Dirichlet boundary condition for time-dependent complex partial differential equations and its application to the nonlinear Schrödinger equation, SIAM J. Sci. Comput. **36**, A1 (2014).